

Controllability Of Brain Networks

Shi Gu^{1,2}, Fabio Pasqualetti³, Matthew Cieslak⁴, Scott T. Grafton⁴, Danielle S. Bassett^{2,5,*}

¹*Applied Mathematics and Computational Science Graduate Group, University of Pennsylvania, Philadelphia, PA, 19104, USA*

²*Complex Systems Group, Department of Bioengineering, University of Pennsylvania, Philadelphia, PA, 19104, USA*

³*Department of Mechanical Engineering, University of California, Riverside, CA, 92521, USA*

⁴*Department of Psychological and Brain Sciences and UCSB Brain Imaging Center, University of California, Santa Barbara, CA 93106, USA*

⁵*Department of Electrical Engineering, University of Pennsylvania, Philadelphia, PA, 19104, USA*

Cognitive function is driven by dynamic interactions between large-scale neural circuits or networks, enabling behavior. Fundamental principles constraining these dynamic network processes have remained elusive. Here we use network control theory to offer a mechanistic explanation for how the brain moves between cognitive states drawn from the network organization of white matter microstructure. Our results suggest that densely connected areas, particularly in the default mode system, facilitate the movement of the brain to many easily-reachable states. Weakly connected areas, particularly in cognitive control systems, facilitate the movement of the brain to difficult-to-reach states. Areas located on the boundary between network communities, particularly in attentional control systems, facilitate the integration or segregation of diverse cognitive systems. Our results suggest that structural network differences between the cognitive circuits dictate their distinct roles in controlling dynamic trajectories of brain network function.

arXiv:1406.5197v1 [q-bio.NC] 19 Jun 2014

Introduction

Neuroscientific investigations seek to reveal how neural systems perform complex functions, how those systems and functions are altered in disease states, and how therapeutic interventions can be used to redirect these alterations. In essence, all three lines of investigation seek to address how neural systems move along dynamic trajectories: of cognitive function, disease, or recovery. Fundamental and therefore generalizable mechanisms of these movements have remained elusive.

The complexity of neural dynamics stems in part from the architectural complexity of the underlying anatomy. Different components (neurons, cortical columns, brain areas) are linked with one another in complex spatial patterns that enable diverse neural functions. These structural interactions can be represented as a graph or network, where component parts form the nodes, and where anatomical links form the edges between nodes. The architecture of these networks displays fascinating heterogeneous features that play a role in neural function¹, development², disease³, and sensitivity to rehabilitation⁴. Despite these recent discoveries, how these architectural features constrain neural dynamics in any of these phenomena is far from understood.

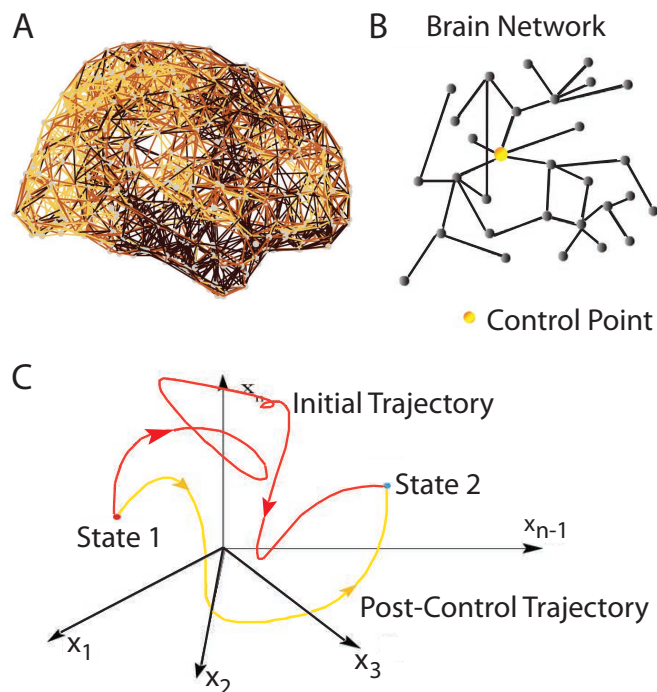


Figure 1: **Conceptual Schematic.** From brain networks (A), we can estimate control points (B) whose activity can move the brain into new dynamic trajectories (referred to as ‘post-control trajectories’) that traverse diverse cognitive functions (C).

Here we capitalize on recent theoretical advances in *network control theory* to quantify the role of structural network organization on the dynamic trajectories of neural systems. Control of

a network refers to the ability to manipulate local interactions of dynamic components to drive the global network along a desired trajectory, meaning a path traversing diverse system states. We postulate that the regulation of cognitive function is driven by a network-level control process akin to those utilized in other biological, technological, cyberphysical, and social systems. In this view, particular nodes (brain regions) at critical locations within the anatomical network topology act as drivers that are able to move the system (brain) into specific modes of action (cognitive functions). While not previously applied to neuroimaging data, network control theory provides a mathematical framework to investigate how structural features of a network impact controllability of cognitive dynamics.

We exploit network control theory to address two basic questions about how the large-scale circuitry of the human brain constrains its dynamics. First, is the human brain theoretically controllable? Based on the fact that cognitive, disease, and therapeutic processes can all alter the trajectories of brain function, we hypothesize that the brain is theoretically controllable. However, since each of these control processes requires alterations across distributed neural circuits, we conjecture that the brain is difficult to control via localized interventions. Second, which areas of the brain are most influential in constraining or facilitating changes in dynamic trajectories? We hypothesize that brain areas will play differential roles in these processes based on their topographical location within the wider network. Furthermore, because brain regions are organized into known cognitive systems, we postulate that structural differences between cognitive systems will predispose them to different roles in network control.

To address these questions, we predict the dynamic control properties of cognitive function based on independent *structural* properties of the brain. We build structural brain networks from diffusion spectrum imaging (DSI) data acquired in triplicate from 8 healthy human adults. We perform diffusion tractography to estimate the number of streamlines linking $N = 234$ large-scale cortical and subcortical regions extracted from the Lausanne atlas ⁵. We summarize these estimates in a weighted adjacency matrix whose entries reflect the number of streamlines connecting different regions. This construction enables us to examine brain network controllability at both the global and regional levels in individual participants.

Mathematical Models

Dynamic Model of Neural Processes Neural activity evolves through neural circuits as a collection of dynamic processes. These processes can be approximated by linearized generalizations ⁶ of nonlinear models of cortical circuit activity ⁷. To study the control properties of neural processes, we focus on a simplified noise-free linear discrete-time and time-invariant network model:

$$\mathbf{x}(t + 1) = \mathbf{A}\mathbf{x}(t) + \mathbf{B}_{\mathcal{K}}\mathbf{u}_{\mathcal{K}}(t), \quad (1)$$

where $\mathbf{x} : \mathbb{R}_{\geq 0} \rightarrow \mathbb{R}^N$ describes the state (i.e., electrical charge or oxygen level) of brain regions over time, and $\mathbf{A} \in \mathbb{R}^{N \times N}$ is a symmetric and weighted adjacency matrix whose elements A_{ij}

indicate the number of streamlines connecting region i and region j , which we scale to ensure stability of the dynamic process at long time intervals⁸. Note that $A_{ii} = 0$. The input matrix $\mathbf{B}_{\mathcal{K}}$ identifies the control points in the brain $\mathcal{K} = \{k_1, \dots, k_m\}$, where

$$\mathbf{B}_{\mathcal{K}} = [e_{k_1} \quad \cdots \quad e_{k_m}], \quad (2)$$

and e_i denotes the i -th canonical vector of dimension N . The input $\mathbf{u}_{\mathcal{K}} : \mathbb{R}_{\geq 0} \rightarrow \mathbb{R}^m$ denotes the control strategy.

Network Controllability The notion of controllability of a dynamical system introduced by Kalman et al.⁹ refers to the possibility of driving the state of a dynamical system to a specific target state by means of a control input. Classic results in control theory ensure that controllability of the network (1) from the set of network nodes \mathcal{K} is equivalent to the controllability Gramian $\mathbf{W}_{\mathcal{K}}$ being invertible, where

$$\mathbf{W}_{\mathcal{K}} = \sum_{\tau=0}^{\infty} \mathbf{A}^{\tau} \mathbf{B}_{\mathcal{K}} \mathbf{B}_{\mathcal{K}}^{\top} \mathbf{A}^{\tau}. \quad (3)$$

The eigenvalues of the controllability Gramian are a quantitative measure of the degree of controllability of different network configurations and trajectories. The structure of the Gramian itself can be further used to provide systematic guidelines for the selection of control areas in the brain that can optimize different cognitive functions, as we demonstrate in the following section.

Results

Global Controllability We first sought to address the question: “Is the human brain theoretically controllable?”. To answer this question, we computed the eigenvalues of the controllability Gramian for each brain region as control node, and for each of the 24 diffusion imaging scans. We observed that the smallest eigenvalues were consistently greater than 0, which demonstrates that the system is theoretically controllable through a single brain region. While estimated to be nonzero, however, the values of the smallest eigenvalues were extremely small (mean 2.5×10^{-23} , STD 4.8×10^{-23}) with respect to the largest eigenvalues (always greater or equal to 1), indicating that in practice the system is extremely hard to control with interventions localized to any single brain region.

Regional Controllability We next sought to address the question: “Which areas of the brain are most influential in constraining or facilitating changes in dynamic trajectories?”. To address this question, we employ 3 diagnostics of regional controllability developed in network control theory: the average, modal, and boundary controllability. Each of these diagnostics captures a different control goal¹⁰. Average controllability identifies brain areas that can steer the system into many easily reachable states, that is, states that are reachable with limited input energy. Modal controllability identifies brain areas that can steer the system into difficult-to-reach states, that is, states requiring a substantial control effort. Boundary controllability identifies brain areas that can

steer the system into states where different cognitive systems are either decoupled or integrated. For mathematical definitions of these diagnostics, see Materials and Methods.

Average Controllability Average controllability identifies brain areas that can steer the system into many different states. The average controllability is greatest in precuneus, posterior cingulate, superior frontal, paracentral, precentral and subcortical structures (Fig. 2A). These areas are strikingly similar to those reported to be the structural “core” of the human cerebral cortex⁵, which innervate the rest of the network with a high density of connections. In other words, these regions are “hubs”, having high network degree, which is defined as the number of edges emanating from that region. To validate this relationship, we show that the average controllability of all brain regions is strongly correlated with degree (Pearson correlation $r = 0.91$, $p = 8 \times 10^{-92}$; Fig. 2B).

Modal Controllability Modal controllability identifies brain areas that can steer the system into difficult-to-reach states. The modal controllability is greatest in postcentral, supramarginal, inferior parietal, pars orbitalis, medial orbitofrontal, and rostral middle frontal cortices (Fig. 2C). In contrast to areas with high average controllability, areas with high modal controllability are not hubs of the network but instead have low degree. The modal controllability of all brain regions is strongly anti-correlated with degree (Pearson correlation $r = -0.99$, $p = 2 \times 10^{-213}$; Fig. 2D). The inverse relationship between degree and modal controllability is consistent with the notion that difficult-to-reach states require the control of poorly connected areas.

Boundary Controllability Boundary controllability identifies brain areas that can steer the system into states where different cognitive systems are either decoupled or isolated. This control goal complements but differs from those of average and modal controllability. The boundary controllability is greatest in rostral middle frontal, lateral orbitofrontal, frontal pole, medial orbitofrontal, superior frontal, and anterior cingulate cortices (Fig. 2E). In contrast to areas with high average or modal controllability, areas with high boundary controllability are neither hubs nor non-hubs. The boundary controllability of all brain regions is not strongly correlated or strongly anti-correlated with degree (Pearson correlation $r = 0.13$, $p = 0.03$; Fig. 2F).

Regional Controllability of Cognitive Systems Finally, we asked the question “Are control regions differentially located in or between known cognitive systems?”. Drawing from the literature, we formulate 3 specific hypotheses addressing this question. First, based on the fact that average controllability identifies areas of the brain that may be important in steering the system into many easily reachable states, we hypothesize that areas of high average controllability would map on to areas active in the brain’s baseline or “default” state (the resting state), from which the brain smoothly moves to multitudinous task states. In contrast, modal controllability identifies areas of the brain that may be important in steering the system to difficult-to-reach states. We hypothesize

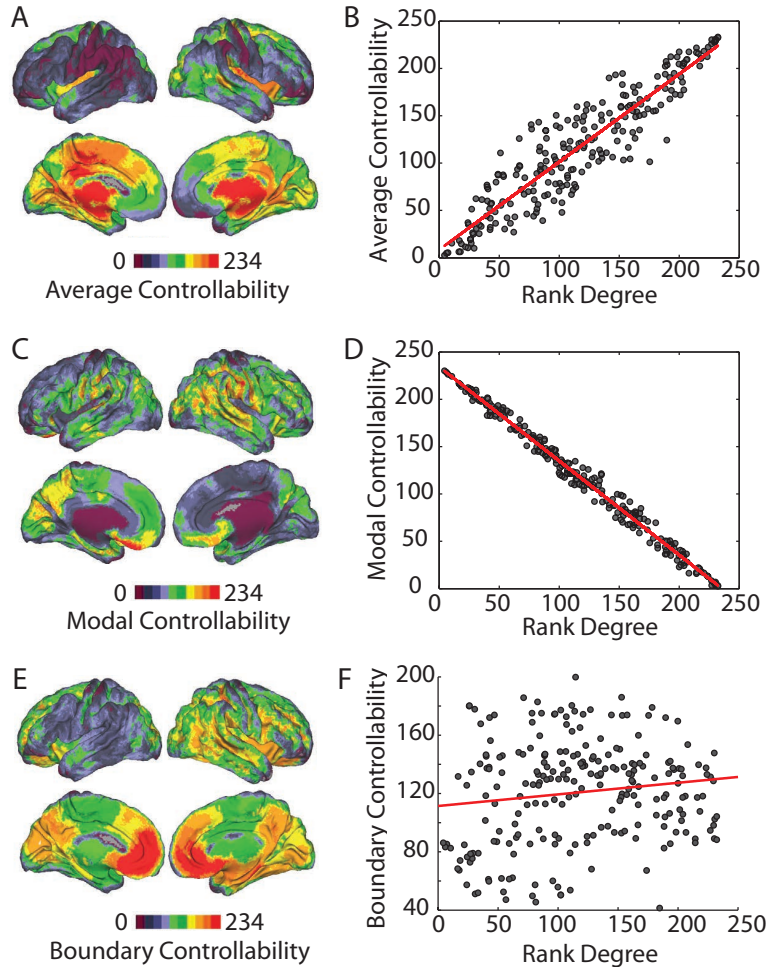


Figure 2: Brain Network Control Properties (A) Average controllability quantifies control to many states. Here we show average controllability values ranked for all brain regions plotted on a surface visualization. Warmer colors indicate larger values of average controllability. (B) Scatter plot of degree (ranked for all brain regions) versus average controllability (Pearson correlation $r = 0.91$, $p = 8 \times 10^{-92}$). (C) Modal controllability quantifies control to difficult-to-reach states. Here we show modal controllability values ranked for all brain regions plotted on a surface visualization. (D) Scatter plot of degree (ranked for all brain regions) versus modal controllability ($r = -0.99$, $p = 2 \times 10^{-213}$). (E) Boundary controllability quantifies control to decouple or integrate network modules. Here we show boundary controllability values ranked for all brain regions plotted on a surface visualization. (F) Scatter plot of degree (ranked for all brain regions) versus boundary controllability ($r = 0.13$, $p = 0.03$). In panels (A), (C), and (E), warmer colors indicate larger controllability values, which have been averaged over both replicates and subjects. These results are reliable over a range of atlas resolutions (see the SI).

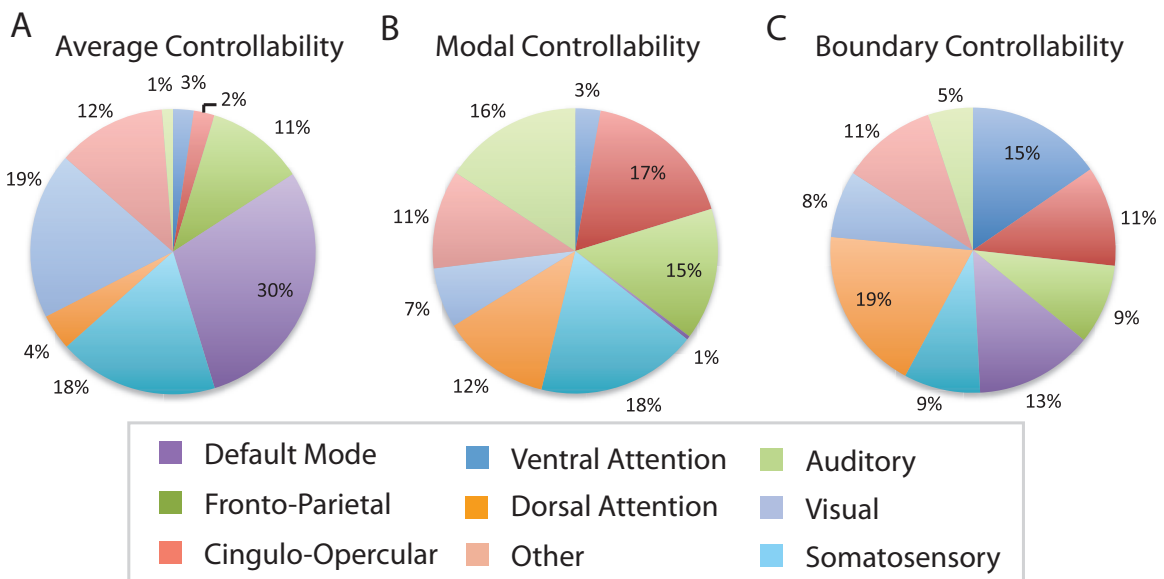


Figure 3: Control Roles of Cognitive Systems Cognitive control hubs are differentially located across cognitive systems. (A) Hubs of average controllability are preferentially located in the default mode system. (B) Hubs of modal controllability are predominantly located in cognitive control systems, including both the fronto-parietal and cingulo-opercular systems. (C) Hubs of boundary controllability are distributed throughout all systems, with the two predominant systems being ventral and dorsal attention systems. Control hubs have been identified at the group level as the 30 regions with the highest controllability values (averaged over replicates and subjects).

that areas of high modal controllability would therefore map on to areas responsible for the brain’s transitions between difficult tasks, specifically executive areas involved in cognitive control. Finally, boundary controllability identifies areas of the brain that can steer the system into states where different cognitive systems are either decoupled or integrated. Because these areas mathematically sit at the boundaries between network communities or putative functional modules, we expect that these areas would map relatively uniformly onto all cognitive systems: each system having a few boundary nodes that might play a role in linking that system to another. However, we also postulate a particular enrichment of the attention systems, based on their role in feature selection, gating, orienting and multi-tasking which constrain integration across other cognitive systems.

To test these hypotheses, we assigned the 234 regions of the Lausanne atlas to the following large-scale cortical networks, which we refer to as “cognitive systems”: auditory, visual, sensorimotor, ventral attention, dorsal attention, default mode, fronto-parietal, and cingulo-opercular. This set of cognitive systems, and the association of regions to these cognitive systems, has previously been extracted from resting state data using a network-based clustering approach ¹¹ and has been widely applied to examine the roles of cognitive systems in task-based and resting-state connectivity ¹²⁻¹⁴ (see the SI for regional attributions to systems).

We find that regions of high controllability are differentially associated with the 8 cognitive systems (Fig. 3). We define the set of high control hubs as the 30 regions with the largest controllability values (averaged over all scans), and we calculate the percent of hubs present from each of the 8 cognitive systems. To correct for system size, we normalize the percentage by the number of regions in a cognitive system. Consistent with our hypotheses, 30% of average control hubs lie in the default mode system, 32% of modal control hubs lie in the fronto-parietal and cingulo-opercular cognitive control systems, and 36% of boundary control hubs lie in the ventral and dorsal attention systems. Our results are qualitatively similar if we choose a larger or smaller set of control hubs (see the SI). These results suggest the presence of a controllability-by-system interaction:

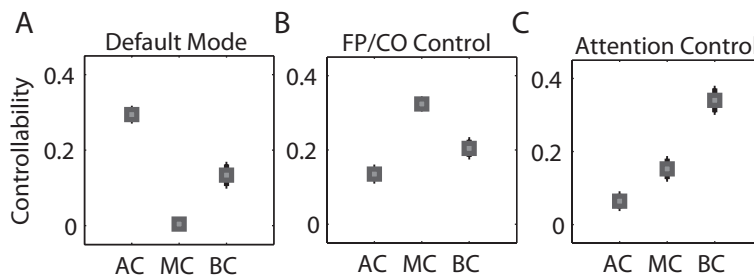


Figure 4: **Differential Recruitment of Cognitive Systems to Network Control** Average controllability (AC), modal controllability (MC), and boundary controllability (BC) hubs are differentially located in default mode (A), fronto-parietal and cingulo-opercular cognitive control (B), and attentional control (C) systems. Values are averaged over the 3 replicates for each individual; error bars indicate standard deviation of the mean over subjects.

certain types of controllability may be utilized or enabled by different cognitive systems. To directly test for this interaction, we extract control hubs for each scan, determine their association with the three hypothesized control systems (default mode, fronto-parietal and cingulo-opercular cognitive control, and attentional control), and quantify the mean controllability value for all hubs in each system (Fig 4). We observe that regions of the default mode system form strong average controllability hubs but weaker modal and boundary controllability hubs. Regions of the cognitive control networks (fronto-parietal and cingulo-opercular) form strong modal controllability hubs and regions of the attentional control networks (ventral and dorsal) form strong boundary controllability hubs. To statistically validate this finding, we perform a repeated measures 2-way Analysis of Variance with cognitive system and controllability diagnostic as categorical factors, and with scan replicate as a repeated measure. The main effect of system is significant ($F(9) = 42.40$; $p = 0$), the main effect of diagnostic is significant ($F(2) = 22.25$, $p = 0.0013$), and the interaction between system and diagnostic is also significant ($F(18) = 39.81$; $p = 0$). These statistics indeed suggest that structural differences between the default mode, cognitive control, and attentional control systems may facilitate their distinct roles in controlling dynamic trajectories of brain network function.

Discussion

The brain is a networked dynamical system that moves between diverse cognitive states to enable complex behaviors. Fundamental principles constraining these dynamic trajectories have remained elusive. Here we use network control theory to offer a mechanistic explanation for how the brain moves between cognitive states drawn from the network organization of white matter microstructure. Our results indicate that densely connected areas are theoretically expected to facilitate the movement of the brain to many easily-reachable states and we show that these areas are preferentially located in the default mode system. Weakly connected areas, predominantly located in cognitive control systems, are theoretically expected to facilitate the movement of the brain to difficult-to-reach states. Finally, areas located on the boundary between network communities, predominantly located in attentional control systems, are theoretically expected to facilitate the integration or segregation of diverse cognitive systems. As a whole, this body of work suggests that structural network differences between the default mode, cognitive control, and attentional control systems dictate their distinct roles in controlling dynamic trajectories of brain network function.

Theoretically Predicted Controllability of Large-Scale Neural Circuitry The relationship between any mathematical measure of controllability, and what it means for a brain to be in control is unknown. Nevertheless, network controllability diagnostics provide theoretical predictions regarding the controllability of large-scale neural circuitry. Using the smallest eigenvalues of the controllability Gramian, we show that structural brain network architecture is theoretically controllable, but pragmatically very difficult to control. The theoretical possibility of controlling the brain from a single region is consistent with a large body of scientific evidence stemming from (i) patient studies that demonstrate that lesions to single brain areas can have dramatic effects on

regional activity, inter-regional connectivity, and by extension cognitive function and behavior¹⁵, and (ii) real-time fMRI studies of neuromodulation that demonstrate that subjects can control the activity of single brain regions to modulate pain perception¹⁶. These findings are consistent with the theoretical expectation that it is possible – with a single input – to move the brain to a single target state. However, our prediction that the brain is pragmatically difficult to control indicates that it is practically impossible to move the brain to *any* target state that we might desire with little control action. This predicted difficulty is consistent with the fact that even complex combinations of drugs, brain stimulation, and cognitive therapies¹⁷ can still fail to right cognitive function when it has gone wrong. These findings suggest that some dynamic trajectories (from disease to health for example) are extremely difficult and practically impossible, particularly from single inputs to single brain areas. The complexity of cognitive function and its underlying mechanisms, illustrated by control difficulty, calls for new tools to quantify and understand which trajectories are amenable to control, thereby informing the use of targeted therapies including brain stimulation¹⁸.

The Role of Hubs in Brain Control We can study brain controllability either globally, as described above, or locally. Network control theory posits the diagnostic of average controllability as a quantification of a node’s role in moving the system to many easily reachable states. We show that brain regions with high average controllability tend to be areas with a large number of white matter streamlines connecting them to the rest of the network – that is, network hubs. These hubs tend to be located in areas of the default mode system. This suggests that the brain has a baseline, resting state organization which is optimized to allow the brain to move to a large number of easily reachable states. Regions of high average controllability, which have the greatest predicted influence in moving the brain to this plethora of states, are highly active at rest in the default mode network. If we assume that the brain has been optimized over evolutionary time scales to maximally enable a complex functional battery^{1,19}, these results suggest the tantalizing possibility that the large majority of complex functions performed by the brain are easily reachable from the default mode state. The few functions which might be difficult to reach from the default mode state may utilize alternative control mechanisms, including modal and boundary control.

The fact that structural hubs, particularly in the default mode network, play such a striking role in brain network controllability may help to explain the growing body of evidence indicating that disease states can preferentially target hub areas³. *In silico* studies suggest that lesions to highly structurally connected areas have a greater impact on ensuing functional connectivity than lesions to sparsely connected areas²⁰. Moreover, alterations to default mode hubs are associated with drastic changes in cognitive function associated with normative aging²¹ and neurodegenerative disorders like Alzheimer’s²². Our results provide a mechanistic explanation for these findings by suggesting that hubs form key control points in brain networks; alterations to hub regions can therefore have disproportionately high impacts on system function.

The Role of Weak Connections in Brain Control While our results demonstrate that hubs are theoretically implicated in moving the brain to many easily reachable states, weakly connected areas are critical for moving the brain to difficult-to-reach states. We observe that these modal

control points, while distributed across the brain, tend to be predominantly located in cognitive control systems including the fronto-parietal and cingulo-opercular networks. These two systems are characterized by different functional connectivity patterns at rest¹¹ and are thought to support distinct functional roles within the general area of cognitive control²³: task-switching²⁴ and task-set maintenance²⁵, respectively. Our results suggest a fundamental underlying mechanism of cognitive control: brain regions sparsely interconnected with the rest of the brain are critically important for moving the system into difficult-to-reach states. This theoretical hypothesis is consistent with the increased engagement of the cognitive control system in highly effortful tasks²⁶.

More generally, the fact that weak connections play a critical role in system dynamics is one that has traditionally received little attention^{27,28}. However, recent work has begun to demonstrate the relevance of weak connections for both cognitive function and psychiatric disease. For example, the topology of weak connections in resting state fMRI could be used to classify healthy volunteers versus schizophrenia patients, while the topology of strong connections could not²⁹. Moreover, in healthy individuals, the topology of weak connections more accurately correlates with intelligent quotients than the topology of strong connections^{30,31}. These findings challenge the traditional view of a prominent role of strong connections in brain dynamics. Our results provide a mechanistic rationale for the importance of weak connections, which are theoretically critical in enabling a system to move to difficult-to-reach states, which may include high performance states (such as measured by IQ) or altered performance states (such as those present in psychiatric conditions).

The Role of Community Structure in Brain Control In addition to the two mechanisms that enable trajectories to (i) many easily reachable states, and (ii) a few difficult to reach states, networked systems often utilize a third mechanism – boundary controllability – which enables the segregation or integration of network modules. Modular structure has been reported in structural³², functional³³, and dynamic³⁴ brain networks. In resting state connectivity studies, these modules have been linked to known cognitive systems¹¹. Our results suggest that a widely distributed set of brain areas across all of these systems enables segregation and integration of putative cognitive modules. We also observe a particular enrichment of boundary control hubs in dorsal and ventral attentional systems, suggesting that attentional control may be implemented by boundary control strategies integrating or segregating disparate cognitive systems. Such a theoretical prediction is supported by evidence that attentional control integrates different cognitive functions^{35,36}, and that disconnections of attentional networks is accompanied by extensive cognitive deficits^{37,38}.

Methodological Considerations The controllability diagnostics that we report and utilize here are highly reliable across multiple scanning sessions (see SI), indicating their potential use in explaining individual differences in cortical function. Moreover, the anatomical distribution of controllability diagnostics is consistent across 5 parcellation schemes segregating the brain into 83, 129, 234, 463, and 1015 regions of interest (see SI), suggesting that these measures are robust quantifications of brain dynamics.

Conclusion A fundamental understanding of the principles by which the brain transitions between diverse cognitive states enabling behavior would necessarily have far-reaching implications for basic cognitive neuroscience and applications in myriad clinical domains. Our results suggest that structural design could underlie basic cognitive control processes, via the fundamental mechanism of network controllability. These findings lay the groundwork for future studies examining relationships between individual differences in network controllability diagnostics and behavioral, cognitive, clinical, and genetic variables.

Methods

Data Acquisition and Preprocessing Diffusion spectrum images (DSI³⁹) were acquired for a total of 8 subjects in triplicate (mean age 27 ± 5 years, 2 female, 2 left handed) along with a $T1$ weighted anatomical scan at each scanning session⁴⁰. DSI scans sampled 257 directions using a $Q5$ half shell acquisition scheme with a maximum b value of 5000 and an isotropic voxel size of 2.4mm. We utilized an axial acquisition with the following parameters: $TR = 11.4s$, $TE = 138ms$, 51 slices, FoV (231,231,123 mm). All participants volunteered with informed consent in accordance with the Institutional Review Board/Human Subjects Committee, University of California, Santa Barbara.

DSI data were reconstructed in DSI Studio (www.dsi-studio.labsolver.org) using q -space diffeomorphic reconstruction (QSDR)⁴¹. QSDR first reconstructs diffusion weighted images in native space and computes the quantitative anisotropy (QA) in each voxel. These QA values are used to warp the brain to a template QA volume in MNI space using the SPM nonlinear registration algorithm. Once in MNI space, spin density functions were again reconstructed with a mean diffusion distance of 1.25mm using three fiber orientations per voxel. Fiber tracking was performed in DSI Studio with an angular cutoff of 55° , step size of 1.0mm, minimum length of 10mm, spin density function smoothing of 0.0, maximum length of 400mm and a QA threshold determined by DWI signal in the CSF. Deterministic fiber tracking using a modified FACT algorithm was performed until 100,000 streamlines were reconstructed for each individual.

Anatomical scans were segmented using FreeSurfer⁴² and parcellated according to the Lausanne 2008 atlas included in the connectome mapping toolkit^{5,43}. A parcellation scheme including 234 regions was registered to the $B0$ volume from each subject's DSI data. The $B0$ to MNI voxel mapping produced via QSDR was used to map region labels from native space to MNI coordinates. To extend region labels through the gray/white matter interface, the atlas was dilated by 4mm. Dilation was accomplished by filling non-labeled voxels with the statistical mode of their neighbors' labels. In the event of a tie, one of the modes was arbitrarily selected. Each streamline was labeled according to its terminal region pair.

Network Controllability Diagnostics We examine 3 diagnostics of controllability utilized in the network control literature: *average controllability*, *modal controllability*, and *boundary controllability*.

bility.

Average Controllability Average controllability of a network – formally defined as $\text{Trace}(\mathbf{W}_{\mathcal{K}}^{-1})$ – equals the average input energy from a set of control nodes and over all possible target states^{44,45}. Motivated by the relation $\text{Trace}(\mathbf{W}_{\mathcal{K}}^{-1}) \geq N^2/\text{Trace}(\mathbf{W}_{\mathcal{K}})$, recent results in the control of networked systems⁴⁶, and the fact that $\mathbf{W}_{\mathcal{K}}$ is close to singularity, we adopt $\text{Trace}(\mathbf{W}_{\mathcal{K}})$ as a measure of the average controllability of a network. Regions with high average controllability are most influential in the control of network dynamics over all different target states.

Modal Controllability Modal controllability refers to the ability of a node to control each evolutionary mode of a dynamical network⁴⁷, and can be used to identify the *least controllable* state from a set of control nodes. Modal controllability is computed from the eigenvector matrix $V = [v_{ij}]$ of the network adjacency matrix \mathbf{A} . By extension from the PBH test⁴⁸, if the entry v_{ij} is small, then the j -th mode is poorly controllable from node i . Following¹⁰, we define $\phi_i = \sum_{j=1}^N (1 - \lambda_j^2(A))v_{ij}^2$ as a scaled measure of the controllability of all N modes $\lambda_1(A), \dots, \lambda_N(A)$ from the brain region i . Regions with high modal controllability are able to control all the dynamic modes of the network, and hence to drive the dynamics towards hard-to-reach configurations.

Boundary Controllability Boundary controllability measures the ability of a set of control nodes to decouple the dynamic trajectories of disjoint brain regions. To evaluate the boundary controllability of different brain regions, we proceed as follows. First, we compute a *robust partition* of the brain network as described in⁴⁹, and we identify the set of N_1 boundary nodes. We assign to these boundary nodes the boundary controllability value of 1. Second, following¹⁰, we determine the two-partition of the least controllable subnetwork from its Fiedler eigenvector^{50,51}, and we identify the additional boundary nodes. We assign to these boundary nodes the boundary controllability value of $(N - N_1)/N$. Finally, we iterate this process until all nodes have been assigned a boundary controllability value.

Average, modal, and boundary controllability each provide a scalar value for each brain region. To enable direct comparison between controllability diagnostics and across different subjects, we perform ranking and normalization steps. In particular, for each of the controllability diagnostics we (i) rank the scalar values for each subject, and (ii) average the ranked values across the subjects.

Acknowledgments

DSB acknowledges support from the Alfred P. Sloan Foundation, the Army Research Laboratory through contract no. W911NF-10-2-0022 from the U.S. Army Research Office, the Institute for Translational Medicine and Therapeutics at Penn, and the National Science Foundation award

#BCS-1441502. SG acknowledges support from the Applied Mathematics and Computational Science Graduate Program at the University of Pennsylvania. MC and STG were supported by PHS Grant NS44393 and the Institute for Collaborative Biotechnologies through grant W911NF-09-0001 from the U.S. Army Research Office. The content is solely the responsibility of the authors and does not necessarily represent the official views of any of the funding agencies.

Supplemental Results

In the main manuscript, we utilize a parcellation of the cortical and subcortical tissue into $N = 234$ different brain regions. This parcellation is in fact part of a wider family of Lausanne atlas parcellations that include the following:

- Scale 33: $N = 83$ brain regions
- Scale 60: $N = 129$ brain regions
- Scale 125: $N = 234$ brain regions
- Scale 250: $N = 463$ brain regions
- Scale 500: $N = 1015$ brain regions

This multi-scale atlas has previously been used to examine the hierarchical nature of brain network topography⁵. In this supplement, we examine the reproducibility of our results obtained using Scale 125 (described in the main manuscript) across the remaining spatial resolutions provided by the other 4 atlases.

Global Controllability Across Spatial Scales We calculated the global controllability of each node in each atlas for each person and scan. We observed that the mean global controllability (averaged across subjects, scans, and nodes) decreases with the spatial scale of the atlas: see Table1. Note: here we report the mean and STD of global controllability diagnostics over brain regions.

Table 1: Global Controllability Diagnostic Values (GC) over the 5 Scales of the Lausanne Atlas Family.

Scale	Number of Nodes	mean GC	STD GC
33	83	2.55×10^{-21}	1.61×10^{-21}
60	129	5.78×10^{-22}	3.88×10^{-22}
125	234	4.52×10^{-23}	3.59×10^{-23}
250	463	7.10×10^{-25}	7.65×10^{-25}
500	1015	2.09×10^{-27}	7.23×10^{-27}

Reproducibility of Controllability Diagnostics Across Spatial Scales In the main manuscript, we show the anatomical distribution of the 3 controllability diagnostics over the $N = 234$ brain regions of the Scale 125 atlas. In Fig. 5 of this supplement, we show that the anatomical distribution of average controllability is visually similar across all 5 spatial scales assessed with the entire Lausanne atlas family. In Fig. 6 and Fig. 7, we show a similar reproducibility of the anatomical distribution of modal and boundary controllability, respectively.

Reproducibility of Degree-Controllability Correlations Across Spatial Scales In the main manuscript, we observed that for Scale 125 ($N = 234$) the degree was strongly positively correlated with the average controllability, strongly negatively correlated with the modal controllability, and neither strongly positively nor strongly negatively correlated with the boundary controllability. In Table 2, we report the correlations between degree and the 3 controllability diagnostics as a function of spatial resolution: from Scale 33 ($N = 83$) to Scale 500 ($N = 1015$). We observe that the degree-controllability correlations reported for Scale 125 are reproducibly observed across the remaining 4 spatial scales, comprising both higher and lower spatial resolutions.

Test-Retest Reliability of Controllability Diagnostics When proposing a new diagnostic of brain network architecture, it is critical to determine the reliability of those diagnostic values across iterative measurement. Here we capitalize on the fact that the same 8 subjects whose data are reported in the main manuscript were imaged over 3 different days. We utilize these iterative scans to assess the test-retest reliability of the 3 controllability diagnostics.

To compare the results among different scans and subjects, we consider the average correlation. Suppose we have n subjects and for each of them we have K scans with corresponding controllability values c_1^i, \dots, c_K^i . The averaged correlation between controllability diagnostic values for subject i and subject j is defined as

$$R_{ij}^B = \frac{\sum_{s=1}^K \sum_{t=1}^K \text{corr}(c_s^i, c_t^j)}{K^2} \tag{4}$$

for subject $i \neq j$ and where s and t index scanning sessions, and corr indicates the calculation of a Pearson correlation coefficient. The average correlation between controllability diagnostic values

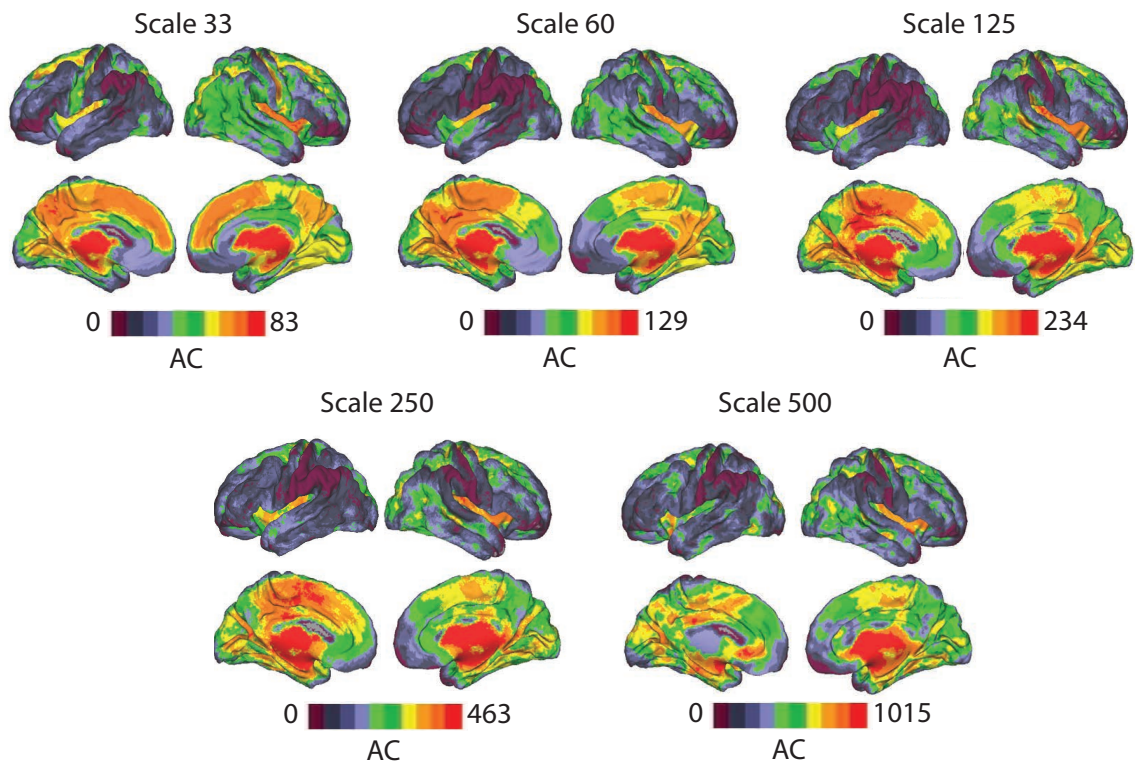


Figure 5: **Average Controllability Across Spatial Scales** Surface visualizations of the ranked average controllability (AC) values over the 5 spatial scales of the Lausanne atlas⁵.

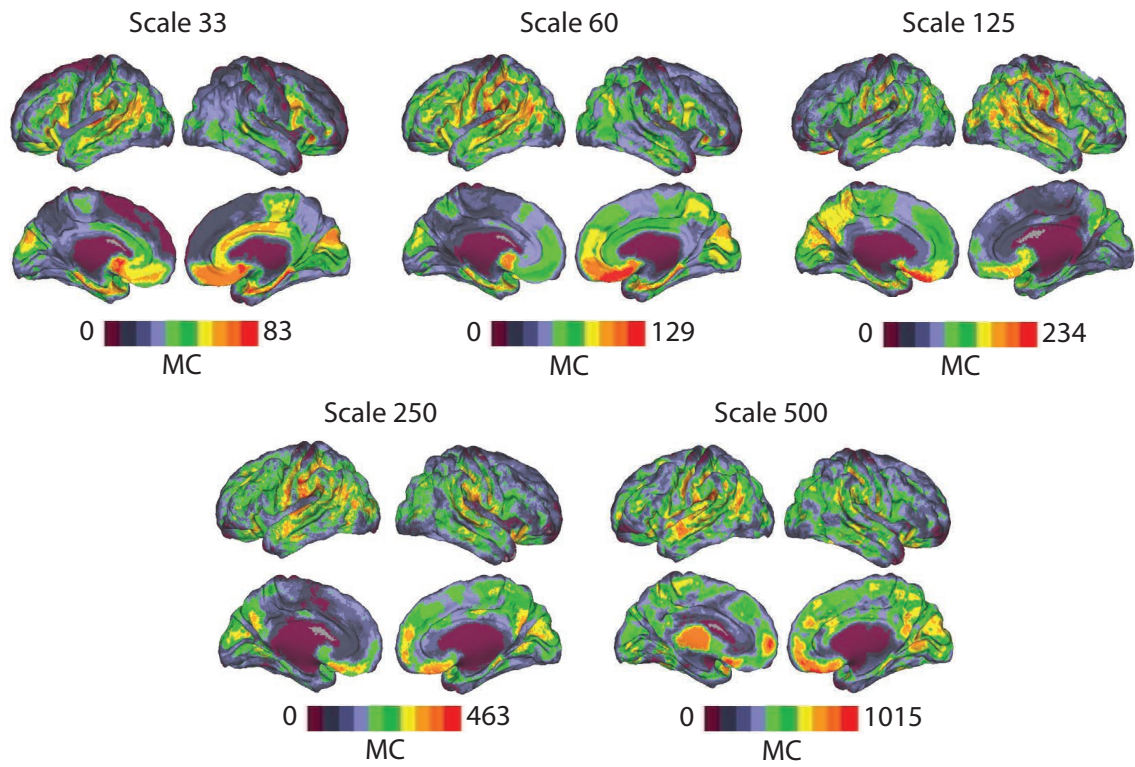


Figure 6: **Modal Controllability Across Spatial Scales** Surface visualizations of the ranked modal controllability (MC) values over the 5 spatial scales of the Lausanne atlas ⁵.

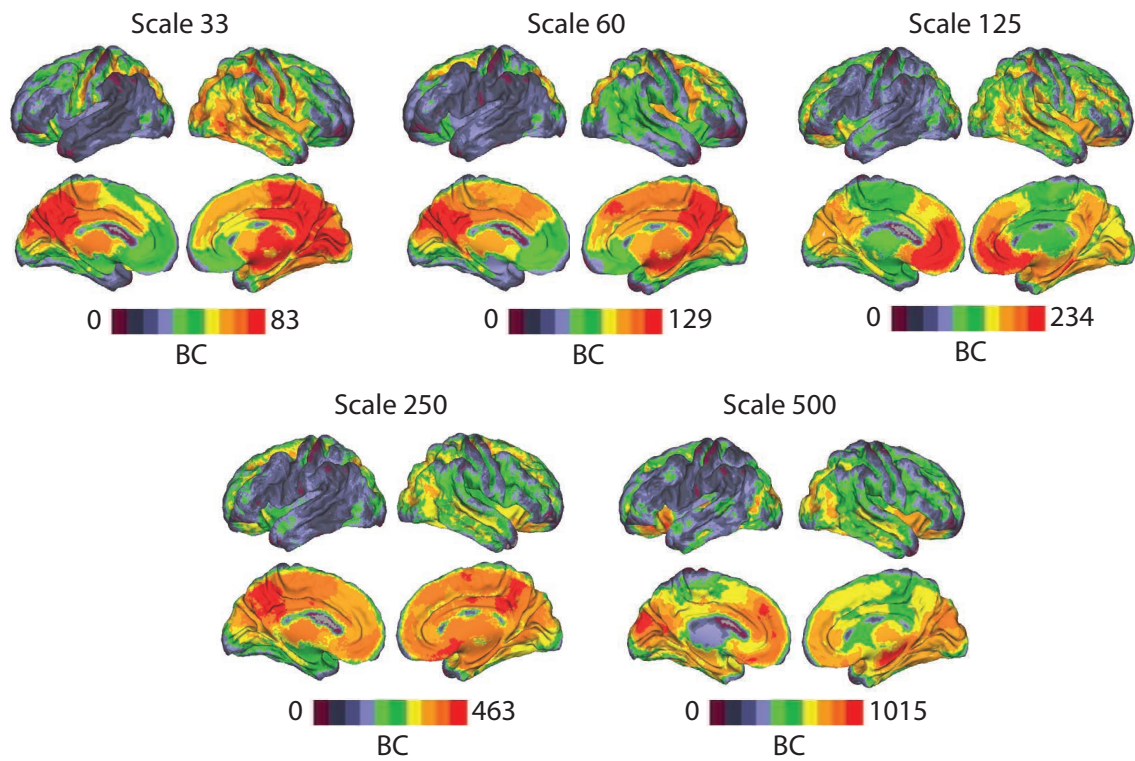


Figure 7: **Boundary Controllability Across Spatial Scales** Surface visualizations of the ranked boundary controllability (BC) values over the 5 spatial scales of the Lausanne atlas⁵.

Table 2: Pearson correlation coefficients r between rank degree, average controllability (AC), boundary controllability (BC), and modal controllability (MC).

	Degree	AC	BC	MC
Scale 33				
Degree	1.0000	0.9764	0.5225	-0.9923
AC	0.9764	1.0000	0.6302	-0.9688
BC	0.5225	0.6302	1.0000	-0.5120
MC	-0.9923	-0.9688	-0.5120	1.0000
Scale 60				
Degree	1.0000	0.9429	0.4733	-0.9912
AC	0.9429	1.0000	0.6262	-0.9320
BC	0.4733	0.6252	1.0000	-0.4806
MC	-0.9912	-0.9320	-0.4806	1.0000
Scale 125				
Degree	1.0000	0.9205	0.1385	-0.9937
AC	0.9205	1.0000	0.1461	-0.9125
BC	0.1385	0.1461	1.0000	-0.1270
MC	-0.9937	-0.9125	-0.1270	1.0000
Scale 250				
Degree	1.0000	0.9114	0.3310	-0.8626
AC	0.9114	1.0000	0.4785	-0.7822
BC	0.3310	0.4785	1.0000	-0.2968
MC	-0.8626	-0.7822	-0.2968	1.0000
Scale 500				
Degree	1.0000	0.9122	0.2709	-0.9962
AC	0.9122	1.0000	0.3637	-0.9042
BC	0.2709	0.3637	1.0000	-0.2366
MC	-0.9962	-0.9042	-0.2366	1.0000

for the same subject across scanning sessions is defined as

$$R_{ii}^W = \frac{\sum_{s \neq t} \text{corr}(c_s^i, c_t^i)}{K(K-1)} \quad (5)$$

for $i = j$. We refer to the quantity R_{ij}^B as the average between-subject correlation and to the quantity R_{ii}^W as the average within-subject correlation.

We report the within- and between-subject correlations for all 3 controllability diagnostics and for global controllability across all 5 spatial scales of the Lausanne atlas family in Tab. 3. We observe that all 3 controllability diagnostics display significantly greater within-subject correlation than between-subject correlation, indicating that these diagnostics are statistically reproducible across scanning sessions and significantly different across individuals. The average and modal controllability display a relatively high mean R (approximately 0.90) and relatively low standard error. While still statistically reproducible across scanning sessions, the boundary controllability displays a lower mean R than the average and modal controllability, and a higher standard error. The global controllability is not reproducible across scanning sessions. These observations are consistently observed across the 5 spatial scales of the Lausanne atlas family of parcellations.

Reproducibility of Control Roles of Cognitive Systems In the main text, we observed that a 30% of average control hubs lie in the default mode system, 32% of modal control hubs lie in the fronto-parietal and cingulo-opercular cognitive control systems, and 34% of boundary control hubs lie in the ventral and dorsal attention systems. Here we demonstrate that these results are qualitatively reproduced for different definitions of control hubs: namely, the 25 nodes with the highest control values (out of a possible 234 nodes), the 30 nodes with the highest control values (as shown in the main manuscript), or the 35 nodes with the highest control values. When control hubs are defined as the top 25 nodes, we observe that 32% of average control hubs lie in the default mode system, 33% of modal control hubs lie in the fronto-parietal and cingulo-opercular systems, and 33% of boundary control hubs lie in the ventral and dorsal attentional systems. When control hubs are defined as the top 35 nodes, we observe that 28% of average control hubs lie in the default mode system, 31% of modal control hubs lie in the fronto-parietal and cingulo-opercular systems, and 32% of boundary control hubs lie in the ventral and dorsal attentional systems. These results demonstrate that the presence of a controllability-by-system interaction is robust to small variation in the choice of the size of the control hub set.

Reproducibility of Differential Recruitment of Cognitive Systems to Network Control In the main text, we observed the presence of a controllability-by-system interaction, and interpreted this as indicative of the possibility that certain types of controllability may be utilized or enabled by different cognitive systems. In particular, we observed that regions of the default mode system form strong average controllability hubs but weaker modal and boundary controllability hubs. Regions of the cognitive control networks (fronto-parietal and cingulo-opercular) form strong modal controllability hubs and regions of the attentional control networks (ventral and dorsal) form strong boundary controllability hubs. Here we demonstrate that these results are qualitatively reproduced

Table 3: Test-Retest Reliability of Controllability Diagnostics: average controllability (AC), boundary controllability (BC), modal controllability (MC) and global controllability (GC).

	AC	BC	MC	GC
Scale 33				
Mean Within	0.9642	0.7250	0.9708	0.0674
Mean Between	0.8966	0.3436	0.9191	0.0501
STE Within	0.0222	0.1279	0.0119	0.0527
STE Between	0.0227	0.2014	0.0168	0.0426
<i>p</i> -value	5.7e-11	2.5e-6	9.2e-12	0.4626
Scale 60				
Mean Within	0.9510	0.6146	0.9519	0.0662
Mean Between	0.8449	0.3465	0.8544	0.0501
STE Within	0.0283	0.1552	0.0199	0.0590
STE Between	0.0333	0.1351	0.0261	0.0387
<i>p</i> -value	4.0e-12	2.8e-6	9.5e-15	0.3076
Scale 125				
Mean Within	0.9404	0.5147	0.9348	0.0782
Mean Between	0.8036	0.1954	0.7900	0.0527
STE Within	0.0298	0.1311	0.0234	0.0508
STE Between	0.0383	0.1638	0.0350	0.0449
<i>p</i> -value	5.3×10^{-14}	1.8×10^{-6}	1.1×10^{-16}	0.1442
Scale 250				
Mean Within	0.9320	0.5192	0.9230	0.0481
Mean Between	0.7751	0.2208	0.7451	0.0391
STE Within	0.0256	0.2012	0.0227	0.0383
STE Between	0.0332	0.2077	0.0267	0.0286
<i>p</i> -value	4.5e-19	4.1e-6	7.8e-26	0.4268
Scale 500				
Mean Within	0.9090	0.4990	0.8982	0.0395
Mean Between	0.7261	0.2367	0.6909	0.0229
STE Within	0.0280	0.1373	0.0263	0.0327
STE Between	0.0338	0.1290	0.0224	0.0241
<i>p</i> -value	1.0e-21	1.4e-6	4.6e-33	0.0864

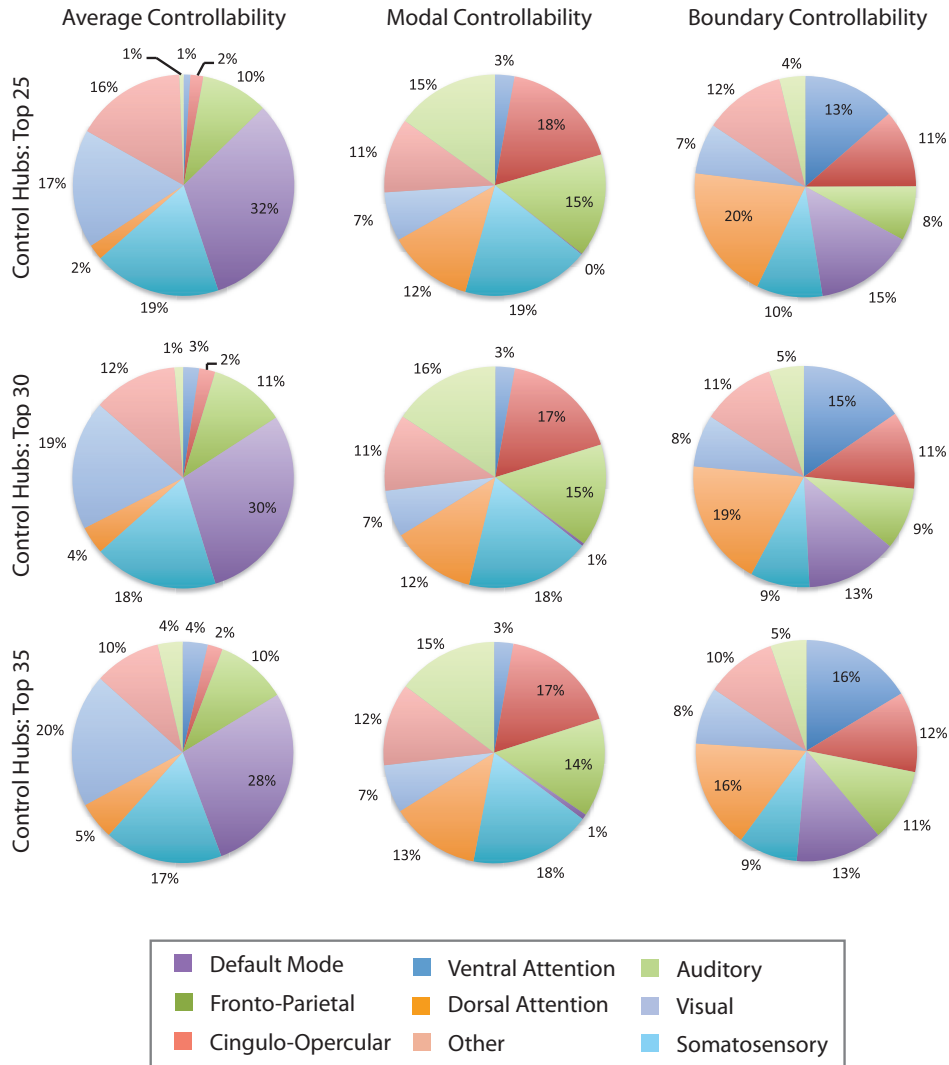


Figure 8: **Control Roles of Cognitive Systems.** Cognitive control hubs are differentially located across cognitive systems. (*Left*) Hubs of average controllability are preferentially located in the default mode system. (*Middle*) Hubs of modal controllability are predominantly located in cognitive control systems, including both the fronto-parietal and cingulo-opercular systems. (*Right*) Hubs of boundary controllability are distributed throughout all systems, with the two predominant systems being ventral and dorsal attention systems. These anatomical distributions are consistent across different definitions of control hubs as either (*Top*) the 25 nodes with the highest control values, (*Middle*) the top 30 nodes with the highest control values, or (*Bottom*) the 35 nodes with the highest control values.

for different definitions of control hubs: namely, the 25 nodes with the highest control values, the 30 nodes with the highest control values (as shown in the main manuscript), or the 35 nodes with the highest control values; see Fig. 9.

In the main text, we validate this finding by performing a repeated measures 2-way Analysis of Variance (ANOVA) with system and controllability diagnostic as categorical factors, and with scan replicate as a repeated measure. Here, we performed the same ANOVA for the case in which control nodes are defined as the 25 nodes with the highest control values or the 35 nodes with the highest control values, and found similar results in both cases: (i) for top 25 nodes, the main effect of system is $F(9) = 43.7716$ ($p = 0$), the main effect of diagnostic is $F(2) = 16.5413$ ($p = 2.0553e - 4$), and the interaction between system and diagnostic is $F(18) = 42.1475$ ($p = 0$); (ii) for the top 35 nodes, the main effect of system is $F(9) = 34.3787$ ($p = 0$), the main effect of diagnostic is $F(2) = 9.7420$ ($p = 0.0022$), and the interaction between system and diagnostic is $F(18) = 36.9762$ ($p = 0$). Consistent with the results reported in the main manuscript, these statistics indeed suggest that structural differences between the default mode, cognitive control, and attentional control systems may facilitate their distinct roles in controlling dynamic trajectories of brain network function. We observe that the weaker control hubs we include in the analysis (i.e., larger number of control hubs), the less significant the relationship to cognitive systems. This suggests that the strong control hubs are significantly associated with cognitive systems but that weak control nodes may not be.

Robustness of Results to Alternative Weighting Schemes There is currently no accepted weighting scheme for constructing anatomical networks from diffusion imaging data. Weighting connections between ROIs based on the number of streamlines connecting them (as estimated by diffusion tractography algorithms) is the most commonly utilized scheme. However, it has been argued that these estimates can be biased by variation in the sizes of the regions under study⁵: large regions may have a higher probability of displays more streamlines than smaller regions. While this potential bias does not appear to drastically alter large-scale topological properties of anatomical networks, its local effects are not well characterized⁵². Our results, based on the number of streamlines, are unlikely to be affected by this potential bias for one key reason: the Lausanne atlas family purposefully attempts to equalize region size, particularly in the higher scales⁵³. Nevertheless, to confirm that our results were robust to an alternative weighting scheme that accounts for region size, we divided each ij^{th} element in the adjacency matrix \mathbf{A} in Scale 125 ($N=234$) by the sum of the sizes of the two regions that it connects to create an alternative adjacency matrix \mathbf{A}' . We then computed the controllability diagnostics and rank degree of \mathbf{A}' for each scan. Similar to our results obtains with the original weighting scheme, we observed that (i) the mean average controllability across the scans is strongly and positively correlated with mean rank degree ($r = 0.97$, $p = 1.43 \times 10^{-150}$), (ii) the mean modal controllability across the scans is strongly and negatively correlated with mean rank degree ($r = -0.96$, $p = 2.51 \times 10^{-130}$), and (iii) the mean boundary controllability is not significantly correlated with mean rank degree ($r = -0.01$, $p = 0.32$). Furthermore, the three network controllability diagnostics are again differentially recruited to known cognitive systems in the same manner as they were for the original weighting scheme (Compare

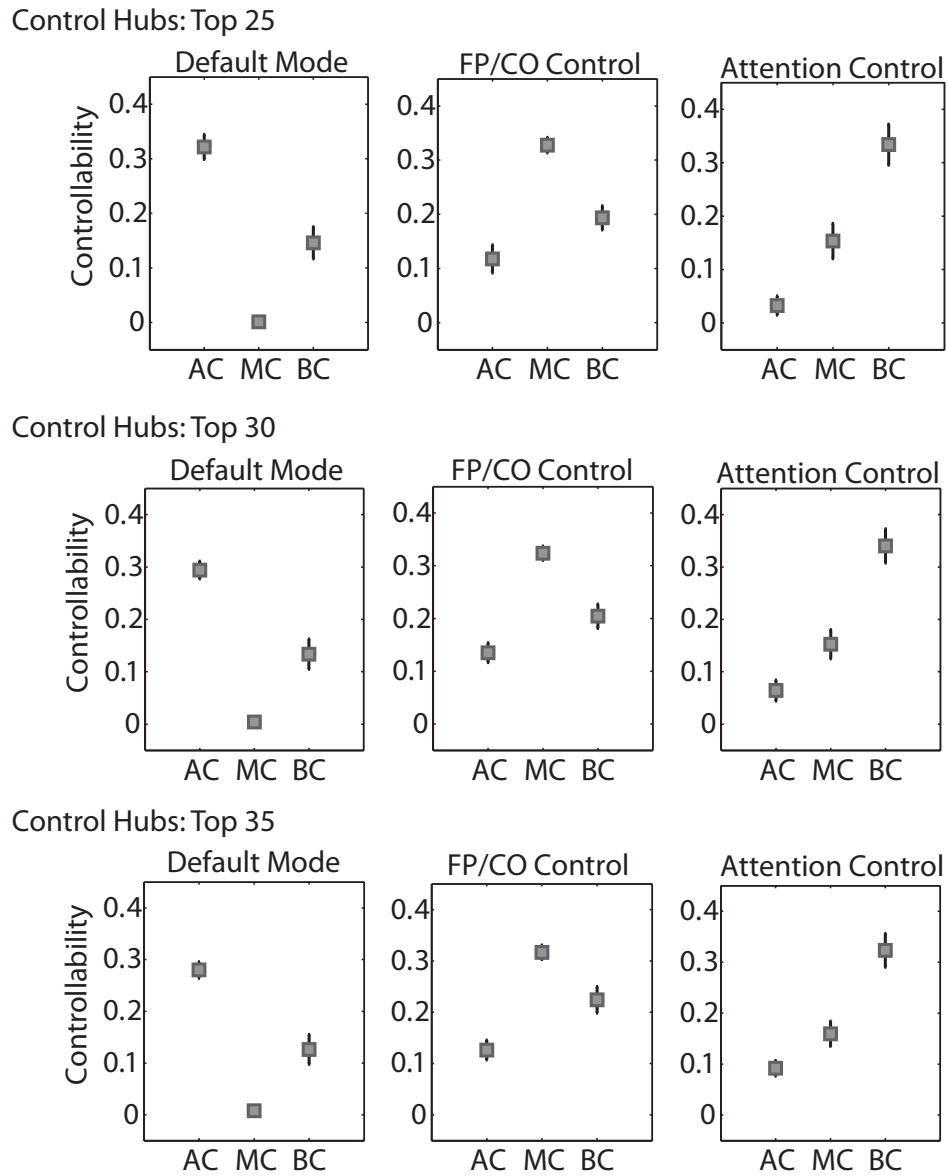


Figure 9: **Differential Recruitment of Cognitive Systems to Network Control.** Average controllability (AC), modal controllability (MC), and boundary controllability (BC) hubs are differentially located in default mode (A), fronto-parietal and cingulo-opercular cognitive control (B), and attentional control (C) systems. These results are consistently observed whether we define control hubs as the 25 nodes with the highest control values (*Top Row*), the 30 nodes with the highest control values (*Middle Row*), or the 35 nodes with the highest control values (*Bottom Row*). Values are averaged over the 3 replicates for each individual; error bars indicate standard deviation of the mean over subjects.

Figure 10 to Figure 4 in the main manuscript). Together, these findings indicate that the results reported in the main manuscript are robust to variations in weighting scheme that include a correction for region size.

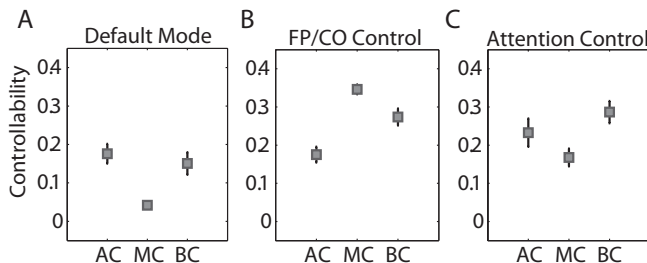


Figure 10: **Differential Recruitment of Cognitive Systems to Network Control** Average controllability (AC), modal controllability (MC), and boundary controllability (BC) hubs are differentially located in default mode (A), fronto-parietal and cingulo-opercular cognitive control (B), and attentional control (C) systems. Values are averaged over the 3 replicates for each individual; error bars indicate standard deviation of the mean over subjects.

Supplementary Discussion

Interpretations Dependent on Model Assumptions Network controllability differs significantly from the static graph theoretical approaches that are increasingly used in studies of human brain connectivity. Network controllability models brain dynamics based on two features: (i) a structural connectivity matrix and (ii) an equation of state defining the dynamics that occur on top of that structure. The theoretical predictions of network controllability diagnostics are therefore dependent on the accuracy of these two features. Here we utilize state-of-the art DSI imaging techniques³⁹ and tractography reconstruction algorithms⁴¹ to estimate white matter streamlines from the medial to lateral surfaces, and to distinguish their crossings⁴⁰. An underlying assumption of this approach is that the number of streamlines is proportional to the strength of structural connectivity; this assumption has important exceptions but is most reasonable for cortico-cortical control, which is the primary area of investigation here (see SI for results from alternative weighting schemes). The equation of state that we utilize is based on extensive prior work demonstrating its utility in predicting resting state functional connectivity⁷ and in providing similar brain dynamics to more complicated models⁶. Nevertheless, this model is simple, and our interpretations are dependent on its assumptions.

Supplemental Methods

Correlation Between Degree and Average Controllability In the main manuscript, we describe a strong correlation between node degree and average controllability for the networks that we study. Here we provide a possible explanation for this effect. Due to the property $\text{Trace}(\mathbf{ABC}) = \text{Trace}(\mathbf{BCA})$, the average controllability with a single control node j equals the j -th diagonal

elements of $(\mathbf{I} - \mathbf{A}^2)^{-1}$. Since A is stable, a first order approximation yields

$$(\mathbf{I} - \mathbf{A}^2)^{-1} \approx \mathbf{I} + \mathbf{A}^2, \quad (6)$$

and the j -th diagonal element of $(\mathbf{I} - \mathbf{A}^2)^{-1}$ is $1 + \sum_{i=1}^N A_{ij}^2$. Since the degree of the j -th node equals $d_j = \sum_{i=1}^N A_{ij}$, a positive correlation between node degree and average controllability is mathematically expected in the networks that we study here.

Lower Bound on the Largest Eigenvalue of the Controllability Gramian In the main manuscript, we show that the smallest eigenvalue of the controllability Gramian is in fact much smaller than its largest counterpart. In fact, the largest eigenvalue of the controllability Gramian is lower bounded by 1. To see this, notice that

$$\lambda_{\max}(W_{\mathcal{K}}) = \lambda_{\max}\left(\sum_{\tau=0}^{\infty} \mathbf{A}^{\tau} \mathbf{B}_{\mathcal{K}} \mathbf{B}_{\mathcal{K}}^{\top} \mathbf{A}^{\tau}\right) \geq \lambda_{\max}\left(\sum_{\tau=0}^0 \mathbf{A}^{\tau} \mathbf{B}_{\mathcal{K}} \mathbf{B}_{\mathcal{K}}^{\top} \mathbf{A}^{\tau}\right) = \lambda_{\max}(\mathbf{B}_{\mathcal{K}} \mathbf{B}_{\mathcal{K}}^{\top}) = 1, \quad (7)$$

where the inequality follows from the fact that $\mathbf{A}^{\tau} \mathbf{B}_{\mathcal{K}} \mathbf{B}_{\mathcal{K}}^{\top} \mathbf{A}^{\tau}$ is positive semi-definite for all τ .

Additional Algorithmic Details for Boundary Control Method In the main manuscript, we briefly describe our method for detecting boundary control points. This method is largely based on the algorithm proposed in ¹⁰. However, for the application to brain networks derived from diffusion tractography, we have made two important modifications to more accurately estimate the initial partition and constrain the boundary point criteria as described in detail below.

Initial Partition The first modification concerns the definitions of the first level subnetworks for which we compute a two-partition based on the Fiedler eigenvector. In initial work, Pasqualetti et al. ¹⁰ suggest computing the Fiedler eigenvector of the adjacency matrix to create first level subnetworks defined by a two-partition. In contrast, we define this first level of subnetworks as composed of network communities, identified by maximizing the modularity quality function ⁵⁴ using a Louvain-like ⁵⁵ locally greedy algorithm ⁵⁶. Our choice is based on extensive recent literature demonstrating that the brain is composed of many subnetworks (not just 2) ^{57,58}, which can be extracted using modularity maximization approaches ³²⁻³⁴, and which correspond to sets of brain areas performing related functions ^{11,32}.

The modularity quality function provides an estimate of the quality of a hard partition of the $N \times N$ adjacency matrix \mathbf{A} into network communities (whereby each brain region is assigned to exactly one network community) ^{54,59-62}

$$Q_0 = \sum_{ij} [A_{ij} - \gamma P_{ij}] \delta(g_i, g_j), \quad (8)$$

where brain region i is assigned to community g_i , brain region j is assigned to community g_j , $\delta(g_i, g_j) = 1$ if $g_i = g_j$ and it equals 0 otherwise, γ is a structural resolution parameter, and P_{ij}

is the expected weight of the edge connecting node i and node j under a specified null model. Maximization of Q_0 yields a hard partition of a network into communities such that the total edge weight inside of communities is as large as possible (relative to the null model and subject to the limitations of the employed computational heuristics, as optimizing Q_0 is NP-hard^{61–63}).

Because the modularity quality function has many near-degeneracies, it is important to perform the optimization algorithm multiple times⁶⁴. We perform 100 optimizations of the Louvain-like locally greedy algorithm⁵⁶ for each adjacency matrix corresponding to a single scan. To distill a single representative partition, we create a consensus partition from these 100 optimizations based on statistical comparison to an appropriate null model⁵⁸.

In a final consideration, we choose a value for the structural resolution parameter γ . The choice $\gamma = 1$ is very common, but it is important to consider multiple values of γ to examine community structure at multiple scales^{61,65,66}. Indeed, recent work has demonstrated that in some networks, a structural resolution parameter value that accurately captures the underlying community structure can be identified by the γ value at which the 100 optimizations produce similar partitions⁵⁸. To quantitatively estimate similarity in partitions, we adopt the z -score of the Rand coefficient⁶⁷. For each pair of partitions α and β , we calculate the Rand z -score in terms of the total number of pairs of nodes in the network M , the number of pairs M_α that are in the same community in partition α , the number of pairs M_β that are in the same community in partition β , and the number of pairs of nodes $w_{\alpha\beta}$ that are assigned to the same community both in partition α and in partition β . The z -score of the Rand coefficient comparing these two partitions is

$$z_{\alpha\beta} = \frac{1}{\sigma_{w_{\alpha\beta}}} w_{\alpha\beta} - \frac{M_\alpha M_\beta}{M}, \quad (9)$$

where $\sigma_{w_{\alpha\beta}}$ is the standard deviation of $w_{\alpha\beta}$. Let the *mean partition similarity* denote the mean value of $z_{\alpha\beta}$ over all possible partition pairs for $\alpha \neq \beta$. Let the *variance of the partition similarity* denote the variance of $z_{\alpha\beta}$ over all possible partition pairs for $\alpha \neq \beta$.

Empirically, we calculated a group adjacency matrix by averaging the adjacency matrices of all subjects and scans. We optimized the modularity quality function 100 times and we computed the mean and variance of the partition similarity for a range of γ values and for all 5 spatial resolutions. Across all atlases, we observed that the mean partition similarity was high and the variance of the partition similarity was low for values of γ ranging between 1.5 and 2. For Scale 125 (the atlas for which we report results in the main manuscript), we observed a maximum mean partition similarity and a minimum variance of partition similarity at $\gamma = 1.6$. We therefore chose to set $\gamma = 1.6$ for the remainder of the analysis in this study.

Boundary Point Criteria The second modification concerns the definition of a boundary point. After calculating the Fiedler eigenvector of a subnetwork to determine a partition of the subnetwork into two communities, we must identify “boundary points”, which are nodes that contain connections to both communities. In the original work by Pasqualetti and colleagues, it was

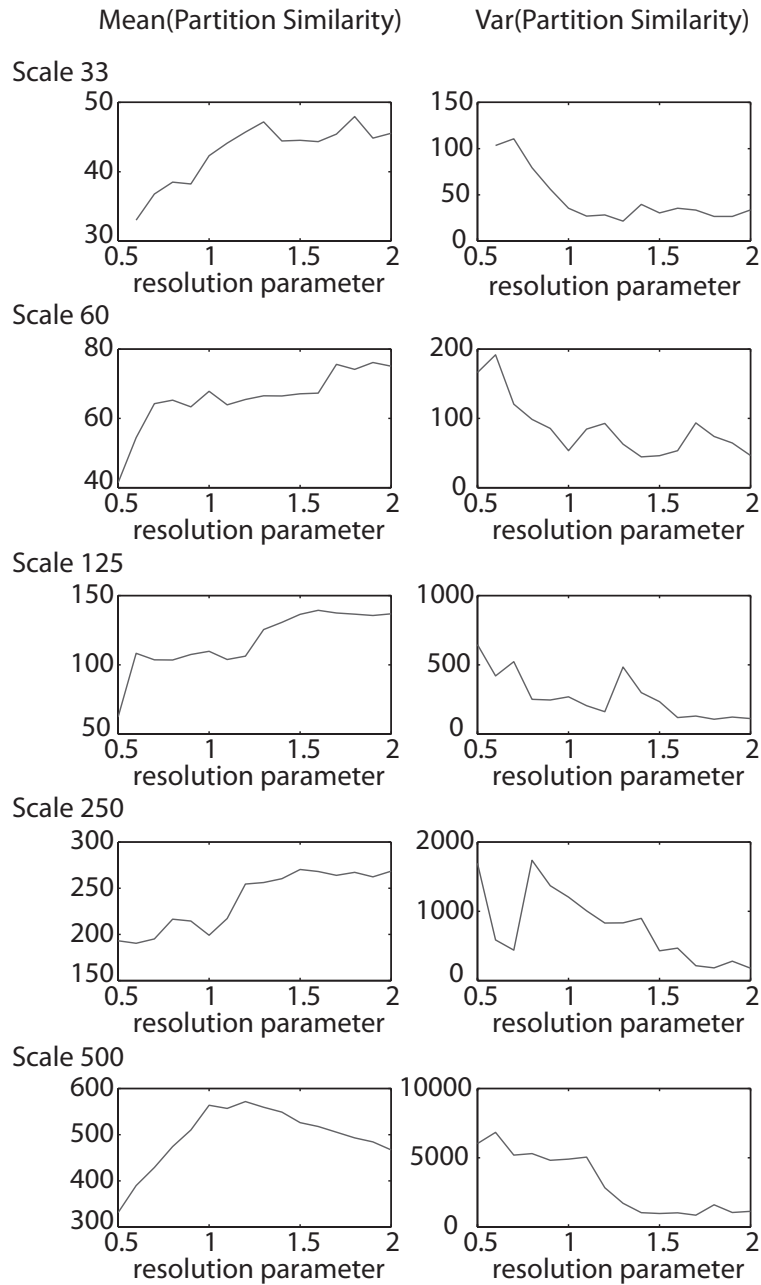


Figure 11: **Partition Similarity As a Function of the Resolution Parameter** Mean (*left*) and variance (*right*) of the partition similarity estimated using the z -score of the Rand coefficient as a function of the structural resolution parameter γ , varies from 0.5 to 2 in increments of 0.1, for the 5 spatial scales of the Lausanne atlas⁵ (*rows*).

suggested that a boundary point was a node with any number of connections to both communities. However, in weighted brain networks we suggest that a more stringent definition is more appropriate for the following reason: practically all nodes in the brain have non-zero weighted connections to both identified communities. Therefore, we instead set a threshold ratio ρ to identify boundary points. Considering the adaptivity to the local measure, we set a threshold ratio ρ instead of a global threshold value. In detail, for a network $G = (V, E)$ with partition $P = (V_1, \dots, V_n)$, a node $i \in V_k$ is called a boundary node if

$$\sum_{l \neq k} a_{kl} \geq \rho \cdot \max(A) \quad (10)$$

where A is the adjacency matrix. Here, $\max(A)$ can be replaced with other statistics and ρ needs to be chosen carefully. If ρ is too small, there will be no effect and the algorithm tends to add the total subnetwork as the set of boundary points. If ρ is too large, there will be only a few points recognized as the boundary points.

In the results described in the main manuscript, we set the threshold ratio to $\rho = 0.2$. To determine whether our results are robust to this choice, we calculate boundary controllability values across all regions in the Scale 125 atlas, for each scan using ρ values that vary between 0.15 and 0.25 in increments of 0.01. We then asked how similar regional control values were for different choices of ρ . Specifically, for any pair of ρ values, we computed the Pearson correlation coefficient between the vectors of regional control values for the two ρ values. We show the results of this analysis in Fig. 12. We observe that the boundary control values are highly similar across choices of ρ (minimum Pearson correlation approximately 0.68, corresponding to a $p = 0$, indicating that our results are robust to small variation in the boundary point criteria threshold).

Final Algorithm Thus, the final algorithm used in the calculation of boundary controllability in this paper can be summarized as follows. We begin with the application of a community detection method to the brain network to extract a partition of brain regions into network communities. We then recursively apply a Fiedler bipartition to add boundary nodes within communities, with the goal of improving the local controllability of the network. At each stage of the algorithm, we define the boundary nodes of the network as the nodes that maintain edges to nodes in other

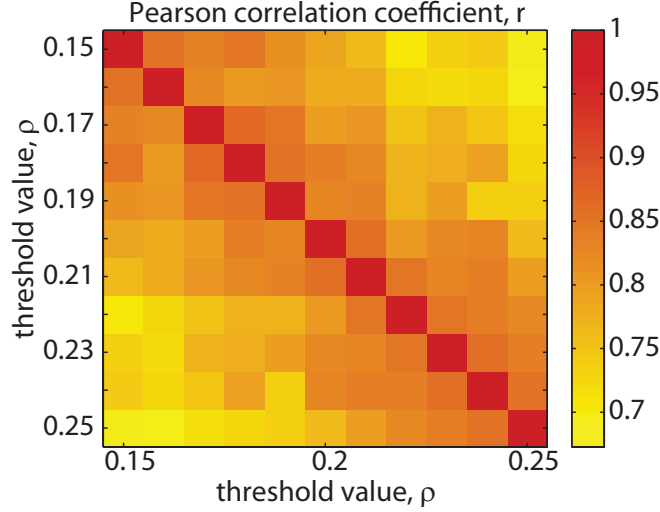


Figure 12: **Effect of Boundary Point Criteria Threshold** Color indicates Pearson correlation coefficient, r , between the vectors of boundary controllability values estimated for pairs of ρ values in the range 0.15–0.25 in increments of 0.01.

communities. Algorithmically, we can write:

Algorithm 1: Algorithm for the Selection of Boundary Control Nodes

Data: Network $G = (V, E)$ with adjacency matrix $A = (a_{ij})$, Number of control nodes m , threshold ratio ρ ;

Result: Control Nodes Index Set \mathcal{K} ;

- 1 Define an empty set of control nodes $\mathcal{K} = \emptyset$;
 - 2 Initialize the partition \mathcal{P} with the result of a community detection algorithm and initialize the boundary nodes set $\mathbf{B} = \emptyset$;
 - 3 Add the boundary points of the initial partition;
 - 4 **while** $|\mathcal{K}| < m$ **do**
 - 5 Select least controllable community $l = \arg \min\{\lambda_{min}(W_{i,\infty}), i = 1, \dots, |\mathcal{P}|\}$;
 - 6 Compute Fiedler two-partition P_f of l -th community;
 - 7 Compute boundary nodes B_f of P_f with the given threshold ratio ρ ;
 - 8 Update partition \mathcal{P} with P_f ;
 - 9 Update control nodes with boundary nodes $\mathcal{K} = \mathcal{K} \cup B_f$;
 - 10 **end**
 - 11 **return** \mathcal{K} .
-

Association of Brain Regions to Cognitive Systems To examine the relationship between controllability diagnostics and cognitive systems, we developed a map of brain areas to a set of cognitive systems previously defined in the literature: the fronto-parietal, cingulo-opercular, dorsal attention, ventral attention, default mode, motor and somatosensory, auditory, visual, subcortical

systems ¹¹. Such a mapping was inspired by a recent paper from Power et al. (2012) who associated 264 brain areas to these cognitive systems, defined by a clustering technique applied to functional brain networks ¹¹. Similar to previous work ¹¹, our association of areas to systems is a gross approximation and it should not be interpreted as indicating that areas have single functions. We use this association only as a pragmatic means to assess whether controllability diagnostics are differentially identified in distributed neural circuits.

The 234 areas examined in the main manuscript were drawn from 42 cortical structures. Here we associate these 42 structures to the set of 9 cognitive systems:

- **Lateral Orbitofrontal** In the Power et al. (2012) decomposition, portions of lateral orbitofrontal cortex (or BA 47) are assigned to default mode, salience, and ventral attention systems. To choose a single association for this region, we turned to the wider literature. In a recent meta-analysis, Zald and colleagues examined the role of medial and lateral orbitofrontal cortex in widespread functional networks ⁶⁸. The lateral orbitofrontal cortex showed co-activations with prefrontal regions and areas involved in cognitive functions including language and memory but not with areas of the default mode, autonomic, and limbic systems. Rothkirch et al. (2012) similarly demonstrated that lateral orbitofrontal cortex appears to be modulated by implicit motivational value, rather than salience ⁶⁹, arguing against its inclusion in the salience system. Anderson and colleagues suggest that lateral orbitofrontal cortex provides a specificity in top-down control of attention in collaboration with dorsolateral prefrontal cortex ⁷⁰. Cognitive system assignment: “Ventral Attention”.
- **Pars Orbitalis** In the Power et al. (2012) decomposition, portions of pars orbitalis (or BA 47) are assigned to default mode, salience, and ventral attention systems. To choose a single association for this region, we turned to the wider literature. The pars orbitalis is a part of the ventrolateral prefrontal cortex, and is known to play a role in cognitive control processes ⁷¹, particularly in conflict adaptation ⁷², inhibition ⁷³, which differ significantly from those enabled by the fronto-parietal network ²³. Cognitive system assignment: “Cingulo-Opercular”.
- **Frontal Pole** In this parcellation scheme, the frontal pole corresponds to portions of BA 9 and 10. These areas form hubs of the fronto-parietal cognitive control system ⁷⁴. Cognitive system assignment: “Fronto-parietal”.
- **Medial Orbitofrontal**. The medial frontal cortex is one of the key hubs of the fronto-parietal network ^{74,75}. Cognitive system assignment: “Fronto-parietal”.
- **Pars Triangularis** In this parcellation scheme, the pars triangularis corresponds to portions of BA 45, and therefore maps to the fronto-parietal cognitive control system ²³. Cognitive system assignment: “Fronto-parietal”.
- **Pars Opercularis** The pars of opercularis (corresponding roughly to BA 44) forms a hub of the cingulo-opercular cognitive control system ²³. Cognitive system assignment: “Cingulo-Opercular”.

- **Rostral Middle Frontal** The rostral middle frontal cortex, corresponding roughly to BA 10, forms a hub of the cingulo-opercular cognitive control system ²³. Cognitive system assignment: “Cingulo-Opercular”.
- **Superior Frontal.** In the Power et al. (2012) decomposition, portions of the superior frontal cortex are predominantly affiliated with the default mode system, consistent with previous literature ⁷⁶⁻⁷⁹. Cognitive system assignment: “Default Mode”.
- **Caudal Middle Frontal** The caudal middle frontal cortex is a prefrontal cortical structure broadly associated with executive function ^{80,81}, top-down control ⁸², and secondary motor processes ^{83,84}. Cognitive system assignment: “Fronto-parietal”.
- **Precentral** The precentral cortex is part of the somatosensory system. Cognitive system assignment: “Somatosensory”.
- **Paracentral** The paracentral cortex is part of the somatosensory system. Cognitive system assignment: “Somatosensory”.
- **Rostral Anterior Cingulate** The anterior cingulate is a hub of the cingulo-opercular network ⁸⁵⁻⁹⁰. Cognitive system assignment: “Cingulo-Opercular”.
- **Caudal Anterior Cingulate** The anterior cingulate is a hub of the cingulo-opercular network ⁸⁵⁻⁹⁰. Cognitive system assignment: “Cingulo-Opercular”.
- **Posterior Cingulate.** The posterior cingulate is a known hub of the default mode system ^{75,91,92}. Cognitive system assignment: “Default Mode”.
- **Isthmus Cingulate** The isthmus cingulate is thought to be a hub of the default mode system ⁹³ and of the limbic system ⁹⁴. Cognitive system assignment: “Default Mode”.
- **Post Central** The postcentral cortex is part of the somatosensory system. Cognitive system assignment: “Somatosensory”.
- **Supramarginal** The supramarginal gyrus appears to play a role in the dorsal ⁹⁵ and ventral ⁹⁶ attention networks, and executive function more broadly ^{97,98}. In the Power et al. (2012) decomposition, this area was assigned to the cingulo-opercular system ¹¹. Cognitive system assignment: “Cingulo-Opercular”.
- **Superior Parietal** The superior parietal cortex plays a role in both the dorsal attention system ^{99,100} and the somatosensory-motor system ¹⁰¹. Cognitive system assignment: “Dorsal Attention”.
- **Inferior Parietal.** The inferior parietal cortex is one of the key hubs of the fronto-parietal network ^{74,75}. Cognitive system assignment: “Fronto-parietal”.
- **Precuneus** The precuneus is a hub of the default mode system ^{102,103}. Cognitive system assignment: “Default Mode”.

- **Cuneus** The cuneus is a part of the visual system ^{99,104,105}. Cognitive system assignment: “Visual”.
- **Pericalcarine** The pericalcarine is a part of the visual system ^{104,106}. Cognitive system assignment: “Visual”.
- **Lateral Occipital** The lateral occipital cortex is a part of the visual system ¹⁰⁷. Cognitive system assignment: “Visual”.
- **Lingual** The lingual gyrus is a part of the visual system ^{104,108}. Cognitive system assignment: “Visual”.
- **Fusiform** The lingual gyrus is a part of the visual system ⁹⁹. Cognitive system assignment: “Visual”.
- **Parahippocampal** The parahippocampal cortex has been associated with many cognitive processes including visuospatial processing and episodic memory ¹⁰⁹. Cognitive system assignment: “Other”.
- **Entorhinal cortex** The entorhinal cortex encodes visual information ¹¹⁰. Cognitive system assignment: “Visual”.
- **Temporal Pole** The temporal pole plays a role in language processing, including naming ¹¹¹, and in social and emotional processing ¹¹². Cognitive system assignment: “Other”.
- **Inferior Temporal** The inferior temporal cortex is associated with visual processing ¹¹³, emotion perception of visual objects ¹¹⁴, and shape recognition ¹¹⁵. Cognitive system assignment: “Visual”.
- **Middle Temporal** The middle temporal cortex is associated with cognitive control processes ¹¹⁶, theory of mind ¹¹⁷, and social cognition ¹¹⁸. Cognitive system assignment: “Other”.
- **Bank of the Superior Temporal Sulcus** The bank of the superior temporal sulcus forms a part of the early cortical auditory network ¹¹⁹. Cognitive system assignment: “Auditory”.
- **Superior Temporal** The superior temporal cortex forms a part of the auditory system ¹²⁰. Cognitive system assignment: “Auditory”.
- **Transverse Temporal** The transverse temporal cortex forms a part of the auditory system ¹²¹. Cognitive system assignment: “Auditory”.
- **Insula.** The insula is one of the key hubs of the fronto-parietal network ^{74,75}. Cognitive system assignment: “Fronto-parietal”.
- **Thalamus.** Cognitive system assignment: “Subcortical”.
- **Caudate.** Cognitive system assignment: “Subcortical”.

- **Putamen.** Cognitive system assignment: “Subcortical”.
- **Pallidum.** Cognitive system assignment: “Subcortical”.
- **Nucleus Accumbens.** Cognitive system assignment: “Subcortical”.
- **Hippocampus.** Cognitive system assignment: “Subcortical”.
- **Amygdala.** Cognitive system assignment: “Subcortical”.
- **Brainstem.** Cognitive system assignment: “Other”.

1. Bullmore, E. & Sporns, O. The economy of brain network organization. *Nat Rev Neurosci* **13**, 336–349 (2012).
2. Feldt, S., Bonifazi, P. & Cossart, R. Dissecting functional connectivity of neuronal microcircuits: experimental and theoretical insights. *Trends Neurosci* **34**, 225–236 (2011).
3. Bassett, D. S. & Bullmore, E. T. Human brain networks in health and disease. *Curr Opin Neurol* **22**, 340–347 (2009).
4. Weiss, S. A. *et al.* Functional brain network characterization and adaptivity during task practice in healthy volunteers and people with schizophrenia. *Front Hum Neurosci* **5** (2011).
5. Hagmann, P. *et al.* Mapping the structural core of human cerebral cortex. *PLoS Biology* **6**, e159 (2008).
6. Fernández Galán, R. On how network architecture determines the dominant patterns of spontaneous neural activity. *PLoS One* **3**, e2148 (2008).
7. Honey, C. J. *et al.* Predicting human resting-state functional connectivity from structural connectivity. *Proc Natl Acad Sci U S A* **106**, 2035–2040 (2009).
8. Horn, R. A. & Johnson, C. R. *Matrix Analysis* (Cambridge University Press, 1985).
9. Kalman, R. E., Ho, Y. C. & Narendra, S. K. Controllability of linear dynamical systems. *Contributions to Differential Equations* **1**, 189–213 (1963).
10. Pasqualetti, F., Zampieri, S. & Bullo, F. Controllability metrics, limitations and algorithms for complex networks. *IEEE Transactions on Control of Network Systems* **1**, 40–52 (2014).
11. Power, J. D. *et al.* Functional network organization of the human brain. *Neuron* **72**, 665–678 (2011).
12. Cole, M. W. *et al.* Multi-task connectivity reveals flexible hubs for adaptive task control. *Nat Neurosci* **16**, 1348–1355 (2013).
13. Power, J. D., Schlaggar, B. L., Lessov-Schlaggar, C. N. & Petersen, S. E. Evidence for hubs in human functional brain networks. *Neuron* **79**, 798–813 (2013).
14. Cole, M. W., Bassett, D. S., Power, J. D., Braver, T. S. & Petersen, S. E. Intrinsic and task-evoked network architectures of the human brain. *Neuron* **In Press** (2014).
15. Grefkes, C. & Fink, G. R. Connectivity-based approaches in stroke and recovery of function. *Lancet Neurol* **13**, 206–216 (2014).
16. deCharms, R. C. *et al.* Control over brain activation and pain learned by using real-time functional MRI. *Proc Natl Acad Sci U S A* **102**, 18626–18631 (2005).
17. Pallanti, S. & Hollander, E. Pharmacological, experimental therapeutic, and transcranial magnetic stimulation treatments for compulsivity and impulsivity. *CNS Spectr* **19**, 50–61 (2014).

18. Johnson, M. D. *et al.* Neuromodulation for brain disorders: challenges and opportunities. *IEEE Trans Biomed Eng* **60**, 610–624 (2013).
19. Bassett, D. S. *et al.* Efficient physical embedding of topologically complex information processing networks in brains and computer circuits. *PloS Comp Biol* **6**, e1000748 (2010).
20. Alstott, J., Breakspear, M., Hagmann, P., Cammoun, L. & Sporns, O. Modeling the impact of lesions in the human brain. *PLoS Comput Biol* **5**, e1000408 (2009).
21. Tomasi, D. & Volkow, N. D. Aging and functional brain networks. *Mol Psychiatry* **17**, 471, 549–558 (2012).
22. Buckner, R. L. *et al.* Cortical hubs revealed by intrinsic functional connectivity: mapping, assessment of stability, and relation to Alzheimer’s disease. *J Neurosci* **29**, 1860–1873 (2009).
23. Elton, A. & Gao, W. Divergent task-dependent functional connectivity of executive control and salience networks. *Cortex* **51**, 56–66 (2014).
24. Stoet, G. & Snyder, L. H. Neural correlates of executive control functions in the monkey. *Trends Cogn Sci* **13**, 228–234 (2009).
25. Shenhav, A., Botvinick, M. M. & Cohen, J. D. The expected value of control: an integrative theory of anterior cingulate cortex function. *Neuron* **79**, 217–240 (2013).
26. Lifshitz, M., Aubert Bonn, N., Fischer, A., Kashem, I. F. & Raz, A. Using suggestion to modulate automatic processes: from Stroop to McGurk and beyond. *Cortex* **49**, 463–473 (2013).
27. Schneidman, E., Berry, M. J. n., Segev, R. & Bialek, W. Weak pairwise correlations imply strongly correlated network states in a neural population. *Nature* **440**, 1007–1012 (2006).
28. Granovetter, M. The strength of weak ties: A network theory revisited. *Sociological Theory* **1**, 201–233 (1983).
29. Bassett, D. S., Nelson, B. G., Mueller, B. A., Camchong, J. & Lim, K. O. Altered resting state complexity in schizophrenia. *Neuroimage* **59**, 2196–2207 (2012).
30. Cole, M. W., Yarkoni, T., Repovs, G., Anticevic, A. & Braver, T. S. Global connectivity of prefrontal cortex predicts cognitive control and intelligence. *J Neurosci* **32**, 8988–8999 (2012).
31. Santarnecchi, E., Galli, G., Polizzotto, N. R., Rossi, A. & Rossi, S. Efficiency of weak brain connections support general cognitive functioning. *Hum Brain Mapp* **Epub ahead of print** (2014).
32. Chen, Z. J., He, Y., Rosa-Neto, P., Germann, J. & Evans, A. C. Revealing modular architecture of human brain structural networks by using cortical thickness from MRI. *Cereb Cortex* **18**, 2374–2381 (2008).

33. Meunier, D., Achard, S., Morcom, A. & Bullmore, E. Age-related changes in modular organization of human brain functional networks. *Neuroimage* **44**, 715–723 (2009).
34. Bassett, D. S. *et al.* Dynamic reconfiguration of human brain networks during learning. *Proc Natl Acad Sci U S A* **108**, 7641–7646 (2011).
35. Corbetta, M. & Shulman, G. L. Control of goal-directed and stimulus-driven attention in the brain. *Nat Rev Neurosci* **3**, 201–215 (2002).
36. Pessoa, L. How do emotion and motivation direct executive control? *Trends Cogn Sci* **13**, 160–166 (2009).
37. Corbetta, M. & Shulman, G. L. Spatial neglect and attention networks. *Annu Rev Neurosci* **34**, 569–599 (2011).
38. Parks, E. L. & Madden, D. J. Brain connectivity and visual attention. *Brain Connect* **3**, 317–338 (2013).
39. Wedeen, V. J., Hagmann, P., Tseng, W. Y. I., Reese, T. G. & Weisskoff, R. M. Mapping complex tissue architecture with diffusion spectrum magnetic resonance imaging. *Magnetic Resonance in Medicine* **54**, 1377–1386 (2005).
40. Cieslak, M. & Grafton, S. T. Local termination pattern analysis: a tool for comparing white matter morphology. *Brain Imaging Behav* **8**, 292–299 (2014).
41. Yeh, F. C. & Tseng, W. Ntu-90: a high angular resolution brain atlas constructed by q -space diffeomorphic reconstruction. *Neuroimage* **58**, 91–99 (2011).
42. Dale, A. M., Fischl, B. & Sereno, M. I. Cortical surface-based analysis. I. Segmentation and surface reconstruction. *NeuroImage* **9**, 179–194 (1999).
43. Gerhard, S. *et al.* The connectome viewer toolkit: an open source framework to manage, analyze, and visualize connectomes. *Frontiers in Neuroinformatics* **5**, 1–15 (2011).
44. Marx, B., Koenig, D. & Georges, D. Optimal sensor and actuator location for descriptor systems using generalized Gramians and balanced realizations. In *American Control Conference*, 2729–2734 (Boston, MA, USA, 2004).
45. Shaker, H. R. & Tahavori, M. Optimal sensor and actuator location for unstable systems. *Journal of Vibration and Control* (2012). URL <http://jvc.sagepub.com/cgi/content/abstract/1077546312451302v1>. <http://jvc.sagepub.com/content/early/2012/07/16/1077546312451302.full.pdf+html>.
46. Summers, T. H. & Lygeros, J. Optimal sensor and actuator placement in complex dynamical networks (2013). ArXiv preprint arXiv:1306.2491.

47. Hamdan, A. M. A. & Nayfeh, A. H. Measures of modal controllability and observability for first-and second-order linear systems. *AIAA Journal of Guidance, Control, and Dynamics* **12**, 421–428 (1989).
48. Kailath, T. *Linear Systems* (Prentice-Hall, 1980).
49. Bassett, D. S. *et al.* Robust detection of dynamic community structure in networks. *Chaos: An Interdisciplinary Journal of Nonlinear Science* **23** (2013).
50. Fortunato, S. Community detection in graphs. *Physics Reports* **486**, 75–174 (2010).
51. Fiedler, M. Algebraic connectivity of graphs. *Czechoslovak Mathematical Journal* **23**, 298–305 (1973).
52. Bassett, D. S., Brown, J. A., Deshpande, V., Carlson, J. M. & Grafton, S. T. Conserved and variable architecture of human white matter connectivity. *Neuroimage* **54**, 1262–1279 (2011).
53. Cammoun, L. *et al.* Mapping the human connectome at multiple scales with diffusion spectrum MRI. *J Neurosci Methods* **203**, 386–397 (2012).
54. Newman, M. E. Modularity and community structure in networks. *Proc Natl Acad Sci U S A* **103**, 8577–8582 (2006).
55. Blondel, V. D., Guillaume, J.-L., Lambiotte, R. & Lefebvre, E. Fast unfolding of communities in large networks. *Journal of Statistical Mechanics: Theory and Experiment* **10**, P1000 (2008).
56. Jutla, I. S., Jeub, L. G. S. & Mucha, P. J. A generalized Louvain method for community detection implemented in MATLAB (2011–2012). URL <http://netwiki.amath.unc.edu/GenLouvain>.
57. Meunier, D., Lambiotte, R. & Bullmore, E. T. Modular and hierarchically modular organization of brain networks. *Front Neurosci* **4**, 200 (2010).
58. Bassett, D. S. & Siebenhuhner, F. *In Multiscale Analysis and Nonlinear Dynamics: From Genes to the Brain*, chap. Multiscale network organization in the human brain (Wiley, 2013).
59. Newman, M. E. & Girvan, M. Finding and evaluating community structure in networks. *Phys Rev E* **69**, 026113 (2004).
60. Newman, M. E. Fast algorithm for detecting community structure in networks. *Phys Rev E* **69**, 066133 (2004).
61. Porter, M. A., Onnela, J.-P. & Mucha, P. J. Communities in networks. *Notices of the American Mathematical Society* **56**, 1082–1097, 1164–1166 (2009).
62. Fortunato, S. Community detection in graphs. *Phys Rep* **486**, 75–174 (2010).

63. Brandes, U. *et al.* On modularity clustering. *IEEE Trans on Knowl Data Eng* **20**, 172–188 (2008).
64. Good, B. H., de Montjoye, Y. A. & Clauset, A. Performance of modularity maximization in practical contexts. *Phys Rev E* **81**, 046106 (2010).
65. Reichardt, J. & Bornholdt, S. Statistical mechanics of community detection. *Phys Rev E* **74**, 016110 (2006).
66. Onnela, J.-P. *et al.* Taxonomies of networks from community structure. *Phys Rev E* **86**, 036104 (2012).
67. Traud, A. L., Kelsic, E. D., Mucha, P. J. & Porter, M. A. Comparing community structure to characteristics in online collegiate social networks. *SIAM Review* **53**, 526–543 (2011).
68. Zald, D. H. *et al.* Meta-analytic connectivity modeling reveals differential functional connectivity of the medial and lateral orbitofrontal cortex. *Cereb Cortex* **24**, 232–248 (2014).
69. Rothkirch, M., Schmack, K., Schlagenhaut, F. & Sterzer, P. Implicit motivational value and salience are processed in distinct areas of orbitofrontal cortex. *Neuroimage* **62**, 1717–1725 (2012).
70. Anderson, J. S., Ferguson, M. A., Lopez-Larson, M. & Yurgelun-Todd, D. Topographic maps of multisensory attention. *Proc Natl Acad Sci U S A* **107**, 20110–20114 (2010).
71. Xiang, H. D., Fonteijn, H. M., Norris, D. G. & Hagoort, P. Topographical functional connectivity pattern in the perisylvian language networks. *Cereb Cortex* **20**, 549–560 (2010).
72. Egner, T. Right ventrolateral prefrontal cortex mediates individual differences in conflict-driven cognitive control. *J Cogn Neurosci* **23**, 3903–3913 (2011).
73. Enriquez-Geppert, S. *et al.* Functional parcellation of the inferior frontal and midcingulate cortices in a flanker-stop-change paradigm. *Hum Brain Mapp* **34**, 1501–1514 (2013).
74. Tu, P. C., Lee, Y. C., Chen, Y. S., Li, C. T. & Su, T. P. Schizophrenia and the brain's control network: aberrant within- and between-network connectivity of the frontoparietal network in schizophrenia. *Schizophr Res* **147**, 339–347 (2013).
75. Stern, E. R., Fitzgerald, K. D., Welsh, R. C., Abelson, J. L. & Taylor, S. F. Resting-state functional connectivity between fronto-parietal and default mode networks in obsessive-compulsive disorder. *PLoS One* **7**, e36356 (2012).
76. Xu, C. P. *et al.* Altered functional connectivity within and between brain modules in absence epilepsy: a resting-state functional magnetic resonance imaging study. *Biomed Res Int* 734893 (2013).

77. Lukoshe, A., White, T., Schmidt, M. N., van der Lugt, A. & Hokken-Koelega, A. C. Divergent structural brain abnormalities between different genetic subtypes of children with Prader-Willi syndrome. *J Neurodev Disord* **5**, 31 (2013).
78. Sun, H. *et al.* Abnormal activity of default mode network in GERD patients. *BMC Neurosci* **14**, 69 (2013).
79. Fang, T. *et al.* Functional connectivity changes in patients with absence epilepsy studied using resting-state functional MRI. *J Clin Neurosci* **20**, 413–418 (2013).
80. Marqués-Iturria, I. *et al.* The interaction effect between BDNF val66met polymorphism and obesity on executive functions and frontal structure. *Am J Med Genet B Neuropsychiatr Genet* **165**, 245–253 (2014).
81. Lopez-Larson, M. P. *et al.* Altered prefrontal and insular cortical thickness in adolescent marijuana users. *Behav Brain Res* **220**, 164–172 (2011).
82. Durazzo, T. C. *et al.* Cortical thickness, surface area, and volume of the brain reward system in alcohol dependence: relationships to relapse and extended abstinence. *Alcohol Clin Exp Res* **35**, 1187–1200 (2011).
83. Verstraete, E., Veldink, J. H., Mandl, R. C., van den Berg, L. H. & van den Heuvel, M. P. Impaired structural motor connectome in amyotrophic lateral sclerosis. *PLoS One* **6**, e24239 (2011).
84. Duffield, T. C. *et al.* Neuropsychological investigation of motor impairments in autism. *J Clin Exp Neuropsychol* **35**, 867–881 (2013).
85. Ninaus, M. *et al.* Neural substrates of cognitive control under the belief of getting neurofeedback training. *Front Hum Neurosci* **7**, 914 (2013).
86. Gratton, C., Lee, T. G., Nomura, E. M. & D’Esposito, M. The effect of theta-burst TMS on cognitive control networks measured with resting state fMRI. *Front Syst Neurosci* **7**, 124 (2013).
87. Vaden, K. I. J. *et al.* The cingulo-opercular network provides word-recognition benefit. *J Neurosci* **33**, 18979–18986 (2013).
88. Becerril, K. E. & Barch, D. M. Conflict and error processing in an extended cingulo-opercular and cerebellar network in schizophrenia. *Neuroimage Clin* **3**, 470–480 (2013).
89. Sestieri, C., Corbetta, M., Spadone, S., Romani, G. L. & Shulman, G. L. Domain-general signals in the cingulo-opercular network for visuospatial attention and episodic memory. *J Cogn Neurosci* **26**, 551–568 (2014).
90. Tu, P. C., Hsieh, J. C., Li, C. T., Bai, Y. M. & Su, T. P. Cortico-striatal disconnection within the cingulo-opercular network in schizophrenia revealed by intrinsic functional connectivity analysis: a resting fMRI study. *Neuroimage* **59**, 238–247 (2012).

91. Khalsa, S., Mayhew, S. D., Chechlacz, M., Bagary, M. & Bagshaw, A. P. The structural and functional connectivity of the posterior cingulate cortex: Comparison between deterministic and probabilistic tractography for the investigation of structure-function relationships. *Neuroimage* **S1053–8119**, 01226–01233 (2013).
92. Leech, R. & Sharp, D. J. The role of the posterior cingulate cortex in cognition and disease. *Brain* **137(Pt 1)**, 12–32 (2014).
93. Zhu, D. C., Majumdar, S., Korolev, I. O., Berger, K. L. & Bozoki, A. C. Alzheimer’s disease and amnesic mild cognitive impairment weaken connections within the default-mode network: a multi-modal imaging study. *J Alzheimers Dis* **34**, 969–984 (2013).
94. Leow, A. *et al.* Impaired inter-hemispheric integration in bipolar disorder revealed with brain network analyses. *Biol Psychiatry* **73**, 183–193 (2013).
95. Schmidt, S. A., Akrofi, K., Carpenter-Thompson, J. R. & Husain, F. T. Default mode, dorsal attention and auditory resting state networks exhibit differential functional connectivity in tinnitus and hearing loss. *PLoS One* **8**, e76488 (2013).
96. Burianová, H., Ciaramelli, E., Grady, C. L. & Moscovitch, M. Top-down and bottom-up attention-to-memory: mapping functional connectivity in two distinct networks that underlie cued and uncued recognition memory. *Neuroimage* **63**, 1343–1352 (2012).
97. Yin, X. *et al.* Anatomical substrates of the alerting, orienting and executive control components of attention: focus on the posterior parietal lobe. *PLoS One* **7**, e50590 (2012).
98. Vasconcelos, L. G. *et al.* The thickness of posterior cortical areas is related to executive dysfunction in Alzheimer’s disease. *Clinics* **69**, 28–37 (2014).
99. Xu, P. *et al.* Different topological organization of human brain functional networks with eyes open versus eyes closed. *Neuroimage* **90**, 246–255 (2014).
100. Sestieri, C., Capotosto, P., Tosoni, A., Luca Romani, G. & Corbetta, M. Interference with episodic memory retrieval following transcranial stimulation of the inferior but not the superior parietal lobule. *Neuropsychologia* **51**, 900–906 (2013).
101. Fabbri, S., Strnad, L., Caramazza, A. & Lingnau, A. Overlapping representations for grip type and reach direction. *Neuroimage* **S1053–8119**, 00162–1 (2014).
102. Cavanna, A. E. & Trimble, M. R. The precuneus: a review of its functional anatomy and behavioural correlates. *Brain* **129**, 564–583 (2006).
103. Sheline, Y. I. & Raichle, M. E. Resting state functional connectivity in preclinical Alzheimer’s disease. *Biol Psychiatry* **74**, 340–347 (2013).
104. Delli Pizzi, S. *et al.* Structural alteration of the dorsal visual network in DLB patients with visual hallucinations: a cortical thickness MRI study. *PLoS One* **9**, e86624 (2014).

105. Collignon, O. *et al.* Impact of blindness onset on the functional organization and the connectivity of the occipital cortex. *Brain* **136**, 2769–2783 (2013).
106. Gaetz, W., Roberts, T. P., Singh, K. D. & Muthukumaraswamy, S. D. Functional and structural correlates of the aging brain: relating visual cortex (V1) gamma band responses to age-related structural change. *Hum Brain Mapp* **33**, 2035–2046 (2012).
107. Bedny, M., Pascual-Leone, A., Dravida, S. & Saxe, R. A sensitive period for language in the visual cortex: distinct patterns of plasticity in congenitally versus late blind adults. *Brain Lang* **122**, 162–170 (2012).
108. Boldt, R. *et al.* Spatial variability of functional brain networks in early-blind and sighted subjects. *Neuroimage* **S1053–8119**, 00219–5 (2014).
109. Aminoff, E. M., Kveraga, K. & Bar, M. The role of the parahippocampal cortex in cognition. *Trends Cogn Sci* **17**, 379–390 (2013).
110. Killian, N. J., Jutras, M. J. & Buffalo, E. A. A map of visual space in the primate entorhinal cortex. *Nature* **491**, 761–764 (2012).
111. Semenza, C. Naming with proper names: the left temporal pole theory. *Behav Neurol* **24**, 277–284 (2011).
112. Olson, I. R., Plotzker, A. & Ezzyat, Y. The Enigmatic temporal pole: a review of findings on social and emotional processing. *Brain* **130**, 1718–1731 (2007).
113. Hirabayashi, T. & Miyashita, Y. Computational principles of microcircuits for visual object processing in the macaque temporal cortex. *Trends Neurosci* **37**, 178–187 (2014).
114. Sabatinelli, D. *et al.* Emotional perception: meta-analyses of face and natural scene processing. *Neuroimage* **54**, 2524–2533 (2011).
115. Tompa, T. & Sáry, G. A review on the inferior temporal cortex of the macaque. *Brain Res Rev* **62**, 165–182 (2010).
116. Noonan, K. A., Jefferies, E., Visser, M. & Lambon Ralph, M. A. Going beyond inferior prefrontal involvement in semantic control: evidence for the additional contribution of dorsal angular gyrus and posterior middle temporal cortex. *J Cogn Neurosci* **25**, 1824–1850 (2013).
117. Rodrigo, M. J., Padrón, I., de Vega, M. & Ferstl, E. C. Adolescents’ risky decision-making activates neural networks related to social cognition and cognitive control processes. *Front Hum Neurosci* **8**, 60 (2014).
118. Hayashi, A. *et al.* Dissociable neural systems for moral judgment of anti- and pro-social lying. *Brain Res* **1556**, 46–56 (2014).
119. Kilian-Hütten, N., Valente, G., Vroomen, J. & Formisano, E. Auditory cortex encodes the perceptual interpretation of ambiguous sound. *J Neurosci* **31**, 1715–1720 (2011).

120. Woods, D. L. & Alain, C. Functional imaging of human auditory cortex. *Curr Opin Otolaryngol Head Neck Surg* **17**, 407–411 (2009).
121. Simon, E. *et al.* Morphometry and localization of the temporal transverse Heschl's gyrus in magnetic resonance imaging: a guide for cortical stimulation of chronic tinnitus. *Surg Radiol Anat* **35**, 115–124 (2013).